by producing IL-22, which promotes subsequent expression of the antimicrobial molecule RegIIIγ by ECs (4, 36, 45). In addition to this, our results describe a previously unknown biological role for ILC3 in the induction and maintenance of intestinal epithelial glycosylation, which leads to the creation of an antipathogenic bacterial platform in the intestine (Fig. 7). Furthermore, epithelial fucosylation contributes to the creation of a cohabitation niche for the establishment of normal commensal microbiota (20, 21). Thus, ILC3-mediated control of epithelial-surface glycosylation might represent a general strategy for regulating the gut microenvironment. Targeted modification of these mechanisms has the potential to provide novel approaches for the control of intestinal infection and inflammation.

Materials and Methods
Mice

C57BL/6 and BALB/c mice were purchased from CLEA Japan (Tokyo, Japan). $Fut2^{-/-}$ and $Il22^{-/-}$ mice (C57BL/6 background) were generated as described previously, and $Id2^{-/-}$ mice were kindly provided by Y. Yokota (33, 46, 47). $Fut2^{-/-}$ mice were crossed onto the BALB/c background for six generations. $Rag2^{-/-}$ mice were kindly provided by F. Alt. $Rag1^{-/-}$; $Rorc^{gfp/gfp}$, $Il6^{-/-}$, $Lta^{-/-}$, $Tcrβ^{-/-}δ^{-/-}$, and $Igh6^{-/-}$ mice were purchased from The Jackson Laboratory. Antibiotic-treated mice were fed a cocktail of broad-spectrum antibiotics—namely, ampicillin (1 g/L; Sigma, Bandai, Japan), vancomycin (500 mg/L; Shionogi, Osaka, Japan), neomycin (1 g/L; Sigma), and metronidazole (1 g/L; Sigma)—or were given these antibiotics in their drinking water, for 4 weeks as previously described (48). These mice were maintained in the experimental animal facility at the University of Tokyo. GF and SFB or L. murinus gnotobiotic mice (BALB/c) were maintained in the GF animal facility at the Yakult Central Institute and at the University of Tokyo. In all experiments, littermates were used at 6 to 10 weeks of age.

Isolation of bacterial DNA

The isolation protocol for bacterial DNA was adapted from a previously described method (49), with some modifications. Bacterial samples in the duodenum and ileum were obtained from mice aged 8 weeks. After removal of PPs and intestinal contents, the intestinal tissues were washed three times with phosphate-buffered saline (PBS) for 10 s each time so as to collect bacteria embedded within the intestinal mucus layer for analysis of microbial composition. These bacteria-containing solutions were centrifuged, and the pellets were suspended in 500 μL of TE buffer (10 mM Tris-HCl, 1 mM EDTA; pH 8.0). Glass beads, Tris-phenol buffer, and 10% sodium dodecyl sulfate (SDS) were added to the bacterial suspensions, and the mixtures were vortexed vigorously for 10 s by using a FastPrep FP100 A (BIO 101). After incubation at 65°C for 10 min, the solutions were vortexed and incubated again at 65°C for 10 min. Bacterial DNA was then precipitated in isopropanol, pelleted by centrifugation, washed in 70%

ethanol, and resuspended in TE buffer. Extracted bacterial DNA was subjected to 16S rRNA gene clone library (50).

16S rRNA gene clone library analyses

For 16S rRNA gene clone library analyses, bacterial 16S rRNA gene sequences were amplified by means of polymerase chain reaction (PCR) with the 27F (5'-AGAGTTTGATCCTGGCTCAG-3') and 1492R (5'-GGTTACCTTGTTACGACTT-3') primers. Amplified 16S rDNA was ligated into the pCR4.0 TOPO vector (Invitrogen, Carlsbad, CA), and the products of these ligation reactions were then transformed into DH-5α-competent cells (TOYOBO, Osaka, Japan). Inserts were amplified and sequenced on an ABI PRISM 3100 Genetic Analyzer (Applied Biosystems, Foster City, CA). The 27F and 520R (5'-ACCGCGGCTGCTGGC-3') primers and a BigDye Terminator cycle sequencing kit (Applied Biosystems) were used for sequencing. Bacterial sequences were identified by means of Basic Local Alignment Search Tool (BLAST) and Ribosomal Database Project searches (50).

Immunohistochemistry

Immunohistochemical analyses were performed as previously described, with some modifications (51). For whole-mount immunofluorescence staining, the mucus layer was removed by flushing the small intestine with PBS; then, the appropriate parts of the small intestine were fixed with 4% paraformaldehyde for 3 hours. After being washing with PBS, whole-mount tissues were stained for at least 3 hours at 4°C with 20 μg/mL UEA-1 conjugated to tetramethylrhodamine B isothiocyanate (UEA-1-TRITC; Vector Laboratories, Burlingame, CA) and 10 μg/mL wheat germ agglutinin (WGA) conjugated to Alexa Fluor 633 (Invitrogen). For whole-mount fluorescence in situ hybridization analysis, we modified the protocol previously described (52). After fixation with 4% paraformaldehyde, intestinal tissues were washed with 1 mL PBS and 100 μL hybridization buffer (0.9 M NaCl, 20 mM Tris-HCl, 0.1% SDS) containing 2 μg EUB338 probe (5'-GCTGCCTCCCGTAGGAGT-3') conjugated to Alexa Fluor 488 (Invitrogen). After overnight incubation at 42°C, the tissues were washed with 1 mL PBS and stained for 3 hours with 10 μg/mL WGA conjugated to Alexa Fluor 633 in PBS. After being washed with PBS, all tissues were analyzed under a confocal laser-scanning microscope (TCS SP2; Leica Microsystems, Wetzlar, Germany).

Cell preparations

A standard protocol was used to prepare intestinal ECs (53). Tissues of the small intestine were extensively rinsed with PBS after removal of PPs. After the intestinal contents had been removed, the samples were opened longitudinally and cut into 1-cm pieces. These tissue pieces were mildly shaken in 1 mM EDTA/PBS for 10 min at 37°C. After passage through a 40-μm mesh filter, intestinal ECs were resuspended in minimum essential medium containing 20% fetal calf serum (FCS). Lamina propria (LP) cells were collected as previously described (54), with

some modifications. Briefly, isolated small intestine was shaken for 40 min at 37°C in RPMI 1640 containing 10% FCS and 1 mM EDTA. Cell suspensions, including intestinal ECs and intraepithelial lymphocytes, were discarded, and the remaining tissues were further digested with continuous stirring for 60 min at 37°C with 2 mg/mL collagenase (Wako) in RPMI 1640 containing 10% FCS. After passage through a 190-μm mesh, the cell suspensions were subjected to Percoll (GE Healthcare) density gradients of 40 and 75%, and the interface between the layers was collected to retrieve LP cells. Stromal cells were identified as CD45⁻ Viaprobe⁻ cells. For fluorescence-activated cell-sorting (FACS) analysis of ILCs, isolated LP cells were further purified by magnetic-activated cell sorting so as to eliminate CD11b⁺, CD11c⁺, and CD19⁺ cells. CD11b⁻ CD11c⁻ CD19⁻ Viaprobe⁻ CD45⁺ LP cells were used to detect ILCs.

Antibodies and flow cytometry

For flow cytometric analysis, isolated intestinal ECs were stained with UEA-1-TRITC, anti-CD45-Pacific blue (PB; Biolegend, San Diego, CA), and Viaprobe (BD Biosciences, East Rutherford, NJ). Viaprobe⁻ CD45⁻ UEA-1⁺ cells were identified as F-ECs. After blocking with anti-CD16/32 (FcγRII/III) (BD Biosciences), the following antibodies were used to stain spleen and LP cells: anti-CD45-PB (Biolegend), anti-CD11b-phycoerythrin (PE), anti-Foxp3-fluorescein isothiocyanate (FITC) (eBioscience, San Diego, CA), anti-CD11c-allophycocyanin (APC), anti-CD11b-FITC, anti-Gr-1-Alexa647, anti-CD3-APC, anti-B220-PE, anti-B220-APC, anti-IgA-FITC, anti-CD4-eFluor450, anti-CD90.2-FITC, anti-IL-17-PE, and anti-IFNγ-FITC (all from BD Biosciences), and Viaprobe. CD11b⁻ CD11c⁻ CD19⁻ LP cells were purified by using anti-CD11b, anti-CD11c, and anti-CD19 MicroBeads (Miltenyi Biotec, Bergisch Gladbach, Germany). The results were obtained by using a FACSAria cell sorter (BD Biosciences) with FlowJo software (TreeStar, Ashland, Oregon).

Intracellular staining of Foxp3 and cytokines

Isolated LP cells were incubated for 4 hours at 37°C with 50 ng/mL phorbol myristate acetate (Sigma), 500 ng/mL ionomycin (Sigma), and GolgiPlug (BD Bioscience) in RPMI 1640 containing 10% FCS and penicillin and streptomycin. After incubation, cells were stained with antibodies against surface antigens for 30 min at 4°C. The cells were fixed and permeabilized with Cytofix/Cytoperm solution (BD Bioscience), and cytokines were stained with the fluorescence-conjugated cytokine antibodies. A Foxp3 staining buffer set (eBioscience) was used for intracellular staining of Foxp3.

Depletion of CD90⁺ ILCs

Depletion of CD90⁺ ILCs was performed as previously described, with some modifications (36). Two hundred and fifty micrograms of a mAb to CD90.2 or an isotype control rat IgG2b (BioXCell, West Lebanon, NH) was given by means of intraperitoneal injection a total of three times at

3-day intervals. Intestinal ECs and LP cells were collected 2 days after the final injection.

Hydrodynamic IL-22 gene delivery system

pLIVE control plasmid (Takara Bio, Shiga, Japan) or IL-22–expressing pLIVE vector (pLIVE-*mIl22*) was introduced into 8-week-old antibiotic-treated C57BL/6 or *Rorc*$^{gfp/gfp}$ mice. Ten micrograms per mouse of plasmid diluted in ~1.5 mL TransIT-EE Hydrodynamic Delivery Solution (Mirus Bio, Madison, WI) was injected via the tail vein within 7 to 10 s. To assess IL-22 expression, serum IL-22 was quantified by means of an enzyme-linked immunosorbent assay (R&D Systems, Minneapolis, MN).

Generation of PP-null mice

mAb to IL-7R (A7R34) was kindly provided by S. Nishikawa. PP-null mice were generated by injecting 600 μg of mAb to IL-7R into pregnant mice on embryonic day 14 (*55*).

In vivo treatment with LTβR-Ig and antibody to IL-22

Neutralization antibody to IL-22 was purchased from eBioscience. Eight-week-old Rag-deficient mice were injected intraperitoneally with antibody to IL-22 a total of five times at 3-day intervals (on days 0, 3, 6, 9, and 12). Plasmid pMKIT-expressing LTβR-Ig and LTβR-Ig treatment was performed as described previously (*56*). Four-week-old C57BL/6 mice were injected intraperitoneally once a week for 3 weeks (on days 0, 7, 14, and 21) with LTβR-Ig fusion protein or control human IgG1 at a dose of 50 μg per mouse. Intestinal ECs were analyzed 3 days after the indicated injection time points.

Adoptive transfer of mixed BM

For mixed BM transfer experiments, *Rorc*$^{gfp/gfp}$ mice were irradiated with two doses of 550 rad each, 3 hours apart. BM cells (1 × 10^7) from *Rorc*$^{gfp/gfp}$ mice was mixed with BM cells (1 × 10^7) from C57BL/6 or *Lta*$^{-/-}$ mice and intravenously injected into irradiated recipient mice. BM chimeric mice were used for experiments 8 weeks after the BM transfer.

Isolation of RNA and real-time reverse transcriptase PCR analysis

Intestinal ECs and subsets of LP cells were sorted with a FACSAria cell sorter (BD Biosciences). The sorted cells were lysed in TRIzol reagent (Invitrogen), and total RNA was extracted in accordance with the manufacturer's instructions. RNA was reverse-transcribed by using a SuperScript VILO cDNA Synthesis Kit (Invitrogen). The cDNA was subjected to real-time reverse transcriptase-PCR (rRT-PCR) by using Roche (Basel, Switzerland) universal probe/primer sets specific for *Lta* (primer F: 5′-tccctcagaagcacttgacc-3′, R: 5′-gagttctgcttgctggggta-3′, probe No. 62), *Ltβ* (primer F: 5′-cctggtgaccctgttgttg-3′, R: 5′-tgctcctgagccaatgatct-3′, probe No. 76), *Il22* (primer F: 5′-tttcctgaccaaactcagca-3′, R: 5′-tctggatgttctggtcgtca-3′, probe No. 17), *Il22r1* (primer F: 5′;-tgctctgttatctgggctacaa-3′, R: 5′-tcaggacacgttggacgtt-3′, probe No. 9), *Il10rβ* (primer F: 5′-attcggagtggggtcaatgtc-3′, R: 5′-gcatctcaggaggtccaatg-

3′, probe No. 29), *Fut2* (primer F: 5′-tgtgacttccaacat-catcc-3′, R: 5′-tctgacagggtttggagctt-3′, probe No. 67), and *Gapdh* (primer F: 5′-tgtccgtcgtggatctgac-3′, R: 5′-cctgcttcaccaccttcttg-3′, probe No. 80). RT-PCR analysis was performed with a Lightcycler II instrument (Roche Diagnostics) to measure the expression levels of specific genes.

Infection with S. typhimurium

Streptomycin-resistant wild-type *S. typhimurium* was isolated from *S. typhimurium* strain ATCC 14028. *Fut2*$^{-/-}$ (BALB/c background) and control littermate mice pretreated with 20 mg of streptomycin 24 hours before infection were given 1 × 10^8 colony-forming units of the isolated *S. typhimurium* via oral gavage. After 24 hours, the mice were dissected, and the cecal contents were collected. Isolated cecum was treated with PBS containing 0.1 mg mL^{-1} gentamicin at 4°C for 30 min so as to kill bacteria on the tissue surface. The cecum was then homogenized and serial dilutions plated in order to determine the number of *S. typhimurium*. Sections of proximal colon were prepared 48 hours after infection. Infiltration of inflammatory cells was confirmed with hematoxylin and eosin staining.

Statistical analysis

Statistical analysis was performed with an unpaired, two-tailed Student's t-test. P values <0.05 were considered statistically significant.

REFERENCES AND NOTES

1. Y. Goto, I. I. Ivanov, Intestinal epithelial cells as mediators of the commensal-host immune crosstalk. *Immunol. Cell Biol.* **91**, 204–214 (2013). doi: 10.1038/icb.2012.80; pmid: 23318659
2. J. Qiu *et al.*, Group 3 innate lymphoid cells inhibit T-cell-mediated intestinal inflammation through aryl hydrocarbon receptor signaling and regulation of microflora. *Immunity* **39**, 386–399 (2013). doi: 10.1016/j.immuni.2013.08.002; pmid: 23954130
3. S. L. Sanos *et al.*, RORgammat and commensal microflora are required for the differentiation of mucosal interleukin 22-producing NKp46+ cells. *Nat. Immunol.* **10**, 83–91 (2009). doi: 10.1038/ni.1684; pmid: 19029903
4. N. Satoh-Takayama *et al.*, Microbial flora drives interleukin 22 production in intestinal NKp46+ cells that provide innate mucosal immune defense. *Immunity* **29**, 958–970 (2008). doi: 10.1016/j.immuni.2008.11.001; pmid: 19084435
5. S. Vaishnava *et al.*, The antibacterial lectin RegIIIγ promotes the spatial segregation of microbiota and host in the intestine. *Science* **334**, 255–258 (2011). doi: 10.1126/science.1209791; pmid: 21998396
6. L. Bry, P. G. Falk, T. Midtvedt, J. I. Gordon, A model of host-microbial interactions in an open mammalian ecosystem. *Science* **273**, 1380–1383 (1996). doi: 10.1126/science.273.5280.1380; pmid: 8703071
7. L. E. Comstock, D. L. Kasper, Bacterial glycans: Key mediators of diverse host immune responses. *Cell* **126**, 847–850 (2006). doi: 10.1016/j.cell.2006.08.021; pmid: 16959564
8. M. J. Coyne, B. Reinap, M. M. Lee, L. E. Comstock, Human symbionts use a host-like pathway for surface fucosylation. *Science* **307**, 1778–1781 (2005). doi: 10.1126/science.1106469; pmid: 15774760
9. L. V. Hooper, J. Xu, P. G. Falk, T. Midtvedt, J. I. Gordon, A molecular sensor that allows a gut commensal to control its nutrient foundation in a competitive ecosystem. *Proc. Natl. Acad. Sci. U.S.A.* **96**, 9833–9838 (1999). doi: 10.1073/pnas.96.17.9833; pmid: 10449780
10. Y. Goto, H. Kiyono, Epithelial barrier: An interface for the cross-communication between gut flora and immune system. *Immunol. Rev.* **245**, 147–163 (2012). doi: 10.1111/j.1600-065X.2011.01078.x; pmid: 22168418
11. K. Terahara *et al.*, Distinct fucosylation of M cells and epithelial cells by Fut1 and Fut2, respectively, in response to intestinal environmental stress. *Biochem. Biophys. Res. Commun.*

404, 822–828 (2011). doi: 10.1016/j.bbrc.2010.12.067; pmid: 21172308
12. E. A. Hurd, S. E. Domino, Increased susceptibility of secretor factor gene Fut2-null mice to experimental vaginal candidiasis. *Infect. Immun.* **72**, 4279–4281 (2004). doi: 10.1128/IAI.72.7.4279-4281.2004; pmid: 15213174
13. A. Franke *et al.*, Genome-wide meta-analysis increases to 71 the number of confirmed Crohn's disease susceptibility loci. *Nat. Genet.* **42**, 1118–1125 (2010). doi: 10.1038/ng.717; pmid: 21102463
14. A. Hazra *et al.*, Common variants of FUT2 are associated with plasma vitamin B12 levels. *Nat. Genet.* **40**, 1160–1162 (2008). doi: 10.1038/ng.210; pmid: 18776911
15. L. Lindesmith *et al.*, Human susceptibility and resistance to Norwalk virus infection. *Nat. Med.* **9**, 548–553 (2003). doi: 10.1038/nm860; pmid: 12692541
16. D. P. McGovern *et al.*, International IBD Genetics Consortium, Fucosyltransferase 2 (FUT2) non-secretor status is associated with Crohn's disease. *Hum. Mol. Genet.* **19**, 3468–3476 (2010). doi: 10.1093/hmg/ddq248; pmid: 20570966
17. D. J. Smyth *et al.*, FUT2 nonsecretor status links type 1 diabetes susceptibility and resistance to infection. *Diabetes* **60**, 3081–3084 (2011). doi: 10.2337/db11-0638; pmid: 22025780
18. B. M. Imbert-Marcille *et al.*, A FUT2 gene common polymorphism determines resistance to rotavirus A of the P[8] genotype. *J. Infect. Dis.* **209**, 1227–1230 (2014). doi: 10.1093/infdis/jit655; pmid: 24277741
19. T. Folseraas *et al.*, Extended analysis of a genome-wide association study in primary sclerosing cholangitis detects multiple novel risk loci. *J. Hepatol.* **57**, 366–375 (2012). doi: 10.1016/j.jhep.2012.03.031; pmid: 22521342
20. P. C. Kashyap *et al.*, Genetically dictated change in host mucus carbohydrate landscape exerts a diet-dependent effect on the gut microbiota. *Proc. Natl. Acad. Sci. U.S.A.* **110**, 17059–17064 (2013). doi: 10.1073/pnas.1306070110; pmid: 24062455
21. P. Rausch *et al.*, Colonic mucosa-associated microbiota is influenced by an interaction of Crohn disease and FUT2 (Secretor) genotype. *Proc. Natl. Acad. Sci. U.S.A.* **108**, 19030–19035 (2011). doi: 10.1073/pnas.1106408108; pmid: 22068912
22. R. B. Sartor, Microbial influences in inflammatory bowel diseases. *Gastroenterology* **134**, 577–594 (2008). doi: 10.1053/j.gastro.2007.11.059; pmid: 18242222
23. J. P. Koopman, A. M. Stadhouders, H. M. Kennis, H. De Boer, The attachment of filamentous segmented micro-organisms to the distal ileum wall of the mouse: A scanning and transmission electron microscopy study. *Lab. Anim.* **21**, 48–52 (1987). doi: 10.1258/002367787780740743; pmid: 3560864
24. K. Suzuki *et al.*, Aberrant expansion of segmented filamentous bacteria in IgA-deficient gut. *Proc. Natl. Acad. Sci. U.S.A.* **101**, 1981–1986 (2004). doi: 10.1073/pnas.0307317101; pmid: 14766966
25. V. Gaboriau-Routhiau *et al.*, The key role of segmented filamentous bacteria in the coordinated maturation of gut helper T cell responses. *Immunity* **31**, 677–689 (2009). doi: 10.1016/j.immuni.2009.08.020; pmid: 19833089
26. I. I. Ivanov *et al.*, Induction of intestinal Th17 cells by segmented filamentous bacteria. *Cell* **139**, 485–498 (2009). doi: 10.1016/j.cell.2009.09.033; pmid: 19836068
27. I. I. Ivanov *et al.*, Specific microbiota direct the differentiation of IL-17-producing T-helper cells in the mucosa of the small intestine. *Cell Host Microbe* **4**, 337–349 (2008). doi: 10.1016/j.chom.2008.09.009; pmid: 18854238
28. C. P. Davis, D. C. Savage, Habitat, succession, attachment, and morphology of segmented, filamentous microbes indigenous to the murine gastrointestinal tract. *Infect. Immun.* **10**, 948–956 (1974). pmid: 4426712
29. Y. Umesaki, H. Setoyama, S. Matsumoto, A. Imaoka, K. Itoh, Differential roles of segmented filamentous bacteria and clostridia in development of the intestinal immune system. *Infect. Immun.* **67**, 3504–3511 (1999).pmid: 10377132
30. I. I. Ivanov *et al.*, The orphan nuclear receptor RORγt directs the differentiation program of proinflammatory IL-17+ T helper cells. *Cell* **126**, 1121–1133 (2006). doi: 10.1016/j.cell.2006.07.035; pmid: 16990136
31. H. Spits *et al.*, Innate lymphoid cells—A proposal for uniform nomenclature. *Nat. Rev. Immunol.* **13**, 145–149 (2013). doi: 10.1038/nri3365; pmid: 23348417
32. H. Spits, J. P. Di Santo, The expanding family of innate lymphoid cells: Regulators and effectors of immunity and tissue remodeling. *Nat. Immunol.* **12**, 21–27 (2011). doi: 10.1038/ni.1962; pmid: 21113163

33. Y. Yokota et al., Development of peripheral lymphoid organs and natural killer cells depends on the helix-loop-helix inhibitor Id2. Nature 397, 702–706 (1999). doi: 10.1038/17812; pmid: 10067894

34. G. Eberl et al., An essential function for the nuclear receptor RORγ(t) in the generation of fetal lymphoid tissue inducer cells. Nat. Immunol. 5, 64–73 (2004). doi: 10.1038/ni1022; pmid: 14691482

35. S. Sawa et al., RORγt⁺ innate lymphoid cells regulate intestinal homeostasis by integrating negative signals from the symbiotic microbiota. Nat. Immunol. 12, 320–326 (2011). doi: 10.1038/ni.2002; pmid: 21336274

36. G. F. Sonnenberg, L. A. Monticelli, M. M. Elloso, L. A. Fouser, D. Artis, CD4(+) lymphoid tissue-inducer cells promote innate immunity in the gut. Immunity 34, 122–134 (2011). doi: 10.1016/j.immuni.2010.12.009; pmid: 21194981

37. S. Buonocore et al., Innate lymphoid cells drive interleukin-23-dependent innate intestinal pathology. Nature 464, 1371–1375 (2010). doi: 10.1038/nature08949; pmid: 20393462

38. G. Pickert et al., STAT3 links IL-22 signaling in intestinal epithelial cells to mucosal wound healing. J. Exp. Med. 206, 1465–1472 (2009). doi: 10.1084/jem.20082683; pmid: 19564350

39. G. F. Sonnenberg, L. A. Fouser, D. Artis, Functional biology of the IL-22–IL-22R pathway in regulating immunity and inflammation at barrier surfaces. Adv. Immunol. 107, 1–29 (2010). doi: 10.1016/B978-0-12-381300-8.00001-0; pmid: 21034969

40. M. Tsuji et al., Requirement for lymphoid tissue-inducer cells in isolated follicle formation and T cell-independent immunoglobulin A generation in the gut. Immunity 29, 261–271 (2008). doi: 10.1016/j.immuni.2008.05.014; pmid: 18656387

41. P. De Togni et al., Abnormal development of peripheral lymphoid organs in mice deficient in lymphotoxin. Science 264, 703–707 (1994). doi: 10.1126/science.8171322; pmid: 8171322

42. D. Chessa, M. G. Winter, M. Jakomin, A. J. Bäumler, Salmonella enterica serotype Typhimurium Std fimbriae bind terminal α (1,2)fucose residues in the cecal mucosa. Mol. Microbiol. 71, 864–875 (2009). doi: 10.1111/j.1365-2958.2008.06566.x; pmid: 19183274

43. M. Awoniyi, S. I. Miller, C. B. Wilson, A. M. Hajjar, K. D. Smith, Homeostatic regulation of Salmonella-induced mucosal inflammation and injury by IL-23. PLOS One 7, e37311 (2012). doi: 10.1371/journal.pone.0037311; pmid: 22624013

44. I. Godinez et al., T cells help to amplify inflammatory responses induced by Salmonella enterica serotype Typhimurium in the intestinal mucosa. Infect. Immun. 76, 2008–2017 (2008). doi: 10.1128/IAI.01691-07; pmid: 18347048

45. A. V. Tumanov et al., Lymphotoxin controls the IL-22 protection pathway in gut innate lymphoid cells during

46. S. E. Domino, L. Zhang, P. J. Gillespie, T. L. Saunders, J. B. Lowe, Deficiency of reproductive tract α(1,2)fucosylated glycans and normal fertility in mice with targeted deletions of the FUT1 or FUT2 α(1,2)fucosyltransferase locus. Mol. Cell. Biol. 21, 8336–8345 (2001). doi: 10.1128/MCB.21.24.8336-8345.2001; pmid: 11713270

47. K. Kreymborg et al., IL-22 is expressed by Th17 cells in an IL-23-dependent fashion, but not required for the development of autoimmune encephalomyelitis. J. Immunol. 179, 8098–8104 (2007). doi: 10.4049/jimmunol.179.12.8098; pmid: 18056351

48. S. Rakoff-Nahoum, J. Paglino, F. Eslami-Varzaneh, S. Edberg, R. Medzhitov, Recognition of commensal microflora by toll-like receptors is required for intestinal homeostasis. Cell 118, 229–241 (2004). doi: 10.1016/j.cell.2004.07.002; pmid: 15260992

49. T. Matsuki et al., Quantitative PCR with 16S rRNA-gene-targeted species-specific primers for analysis of human intestinal bifidobacteria. Appl. Environ. Microbiol. 70, 167–173 (2004). doi: 10.1128/AEM.70.1.167-173.2004; pmid: 14711639

50. R. Kibe, M. Sakamoto, H. Hayashi, H. Yokota, Y. Benno, Maturation of the murine cecal microbiota as revealed by terminal restriction fragment length polymorphism and 16S rRNA gene clone libraries. FEMS Microbiol. Lett. 235, 139–146 (2004). doi: 10.1111/j.1574-6968.2004.tb09578.x; pmid: 15158273

51. M. H. Jang et al., Intestinal villous M cells: An antigen entry site in the mucosal epithelium. Proc. Natl. Acad. Sci. U.S.A. 101, 6110–6115 (2004). doi: 10.1073/pnas.0400969101; pmid: 15071180

52. T. Obata et al., Indigenous opportunistic bacteria inhabit mammalian gut-associated lymphoid tissues and share a mucosal antibody-mediated symbiosis. Proc. Natl. Acad. Sci. U.S.A. 107, 7419–7424 (2010). doi: 10.1073/pnas.1001061107; pmid: 20360558

53. M. Yamamoto, K. Fujihashi, K. Kawabata, J. R. McGhee, H. Kiyono, A mucosal intranet: Intestinal epithelial cells down-regulate intraepithelial, but not peripheral, T lymphocytes. J. Immunol. 160, 2188–2196 (1998). ; pmid: 9498757

54. N. Ohta et al., IL-15-dependent activation-induced cell death-resistant Th1 type CD8 α β⁺NK1.1⁺ T cells for the development of small intestinal inflammation. J. Immunol. 169, 460–468 (2002). doi: 10.4049/jimmunol.169.1.460; pmid: 12077277

55. H. Yoshida et al., IL-7 receptor α⁺ CD3(-) cells in the embryonic intestine induces the organizing center of Peyer's patches. Int. Immunol. 11, 643–655 (1999). doi: 10.1093/intimm/11.5.643; pmid: 10330270

56. M. Yamamoto et al., Role of gut-associated lymphoreticular tissues in antigen-specific intestinal IgA immunity. J. Immunol. 173, 762–769 (2004). doi: 10.4049/jimmunol.173.2.762; pmid: 15240662
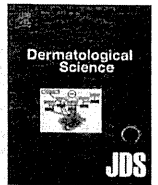
ACKNOWLEDGMENTS

SUPPLEMENTARY MATERIALS

Letter to the Editor

Immediate-type contact hypersensitivity is reduced in interleukin-33 knockout mice

Interleukin-33 (IL-33) is a member of the IL-1 cytokine family, along with IL-1beta and IL-18. IL-33 binds to its receptor ST2 (IL-1RL1), which is expressed by Th2 cells and by various innate immune cells including mast cells and basophils, in which ST2 and the IL-18 receptor α chain, respectively, are predominant [1]. IL-33 stimulates the production of Th2 cytokines by those cells and is involved in various types of inflammation [2]. Recently, we have found that ragweed-induced allergic rhinitis is dependent on IL-33 [3] and mast cells are abundant in the dermis of skin-specific IL-33 transgenic mice [4]. Those prompted us to elucidate the role of IL-33 in cutaneous immediate-type contact hypersensitivity. In this study, we examined hapten-induced immediate-type contact hypersensitivity in IL-33 knockout (KO) mice.

All animal experiments were performed in accordance with the guidelines of the Institutional Animal Care Committee of the Hyogo College of Medicine. WT BALB/c mice (Charles River Laboratories, Yokohama, Japan) and IL-33 KO mice [2] were sensitized on their shaved dorsal skins with 0.5% (wt/vol) 2,4-dinitro-fluorobenzene (DNFB; Sigma, St. Louis, MO), and were repeatedly challenged with 0.2% (wt/vol) DNFB on their left ears and with vehicle only on their right ears once a week (Fig. 1a), as described previously [5]. The ear thickness was measured before and after each challenge using a dial thickness gauge (Ozaki, Tokyo, Japan). No immediate reaction occurred after the first challenge. However, WT mice showed both immediate and delayed-type reactions after the third challenge (Fig. 1b, open squares). In contrast, in IL-33 KO mice the delayed-type reaction remained as reported that IL-33 is unnecessary for T cell-dependent acquired immune responses [6], but the immediate reaction was significantly suppressed (Fig. 1b, closed squares). When only vehicle was applied, no immediate reactions occurred in WT or in IL-33 KO mice, and therefore those reactions were hapten-specific. To determine whether the difference of ear swelling in those mice is related with IgE, we measured serum levels of hapten-specific IgE by ELISA as described previously [7]. However, both IL-33 KO and WT mice showed a strong hapten-specific IgE response (Fig. 1c). Plasma histamine levels, which were measured using an ELISA kit (Immunotech, Marseille, France),

were significantly lower in IL-33 KO mice than in WT mice (Fig. 1d). This result might coincide with the poor immediate hypersensitivity reaction in IL-33 KO mice. Because both mast cells and basophils could be a major source of histamine, we examined the numbers of those cells in the skin just before the third challenge. Toluidine blue staining showed that the number of mast cells in the skin was increased in WT mice, but not in IL-33 KO mice (Fig. 1e and f). In contrast, immunohistochemistry using a murine basophil-specific anti-mMCP-8 antibody (clone TUG8, Biolegend, San Diego, CA) [3] revealed that the number of basophils in the skin was not different between WT and IL-33 KO mice (Fig. 1g and h). Therefore, DNFB-induced mast cell recruitment might be mediated by IL-33 and the difference of ear swelling in the immediate hypersensitivity reaction might be dependent on the number of mast cells in the skin.

Next, the effect of the hapten DNFB on the localization and/or expression of IL-33 was examined by immunofluorescence (Fig. 2) as described previously [7]. IL-33 was localized in the nuclei of keratinocytes in naïve mouse skin, but the epidermal expression of IL-33 was down-regulated 6 h after the DNFB challenge, and it recovered at 24 h (Fig. 2b). DNFB-induced IL-33 up-regulation was only seen in keratinocytes, not in endothelial cells. Consequently, DNFB may cause the production of IL-33 from keratinocytes, instead of other IL-33 producing cells. The time-course of IL-33 expression suggests that exposure of the epidermis to DNFB may cause the secretion of IL-33 from keratinocytes and thereby elicits a transient decrease in the nuclear IL-33 protein. In turn, real-time PCR revealed that IL-33 mRNA expression increased 6 h after the application of DNFB and returned toward the baseline level at 24 h (Fig. 2c). Such a loss of IL-33 protein with an increase in IL-33 mRNA has been found in nasal epithelial cells in patients with allergic rhinitis [3].

From these results, we propose the following mechanism for immediate contact hypersensitivity. IL-33 is secreted from keratinocytes in response to stimuli such as allergens. IL-33 acts as an alarmin and recruits ST2+ mast cells into the skin. Antigen stimulation then releases a large amount of histamine from the abundant mast cells and triggers immediate contact hypersensitivity. However, further study is necessary to elucidate how IL-33 recruits mast cells into the skin [4,8].
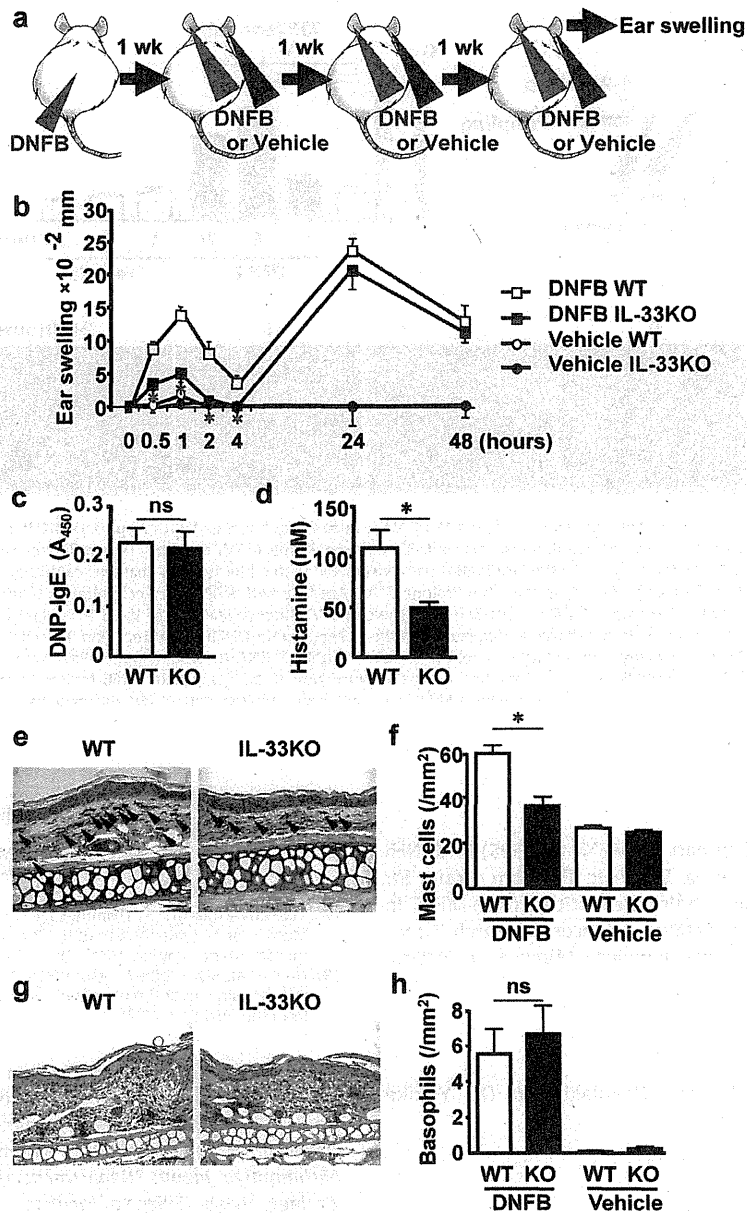
Fig. 1. Immediate contact hypersensitivity is suppressed in IL-33 KO mice. (a) Induction of contact hypersensitivity. WT BALB/c mice or IL-33 KO mice were sensitized on their shaved dorsal skins with 25 μl 0.5% DNFB in a 4:1 acetone/olive oil solution (A/O) in week 0, and were repeatedly challenged with 20 μl 0.2% DNFB in A/O on their left ears or vehicle only on their right ears once a week. wk, week. (b) Time-course of ear thickness in WT and IL-33KO mice after the third challenge. (c) Sera levels of hapten-specific IgE. Sera were sampled 48 h after the third challenge and anti-2,4-dinitrophenol (DNP)-IgE was measured by ELISA. Absorbance at 450 nm (A_{450}) was measured using a microplate spectrophotometer (Benchmark Plus; Bio-Rad, Hercules, CA). WT mouse serum was used as a negative control (blank absorbance). (d) Histamine concentration in plasma measured by ELISA. (e) Toluidine blue staining of WT and IL-33 KO skins. Arrowheads indicate mast cells. Bar, 50 μm. (f) The number of mast cells in the skin was calculated as the mean of 6 microscopic fields. (g) Immunohistochemistry of basophils in the skin from WT and from IL-33 KO mice. Bar, 50 μm. (h) The number of basophils in the skin was calculated as the mean of 6 microscopic fields. All data are expressed as means ± SEM (n = 8) and representative data of two independent experiments are shown. *P < 0.05; ns, not significant (unpaired t-test, calculated using PRISM6; GraphPad Software, San Diego, CA).
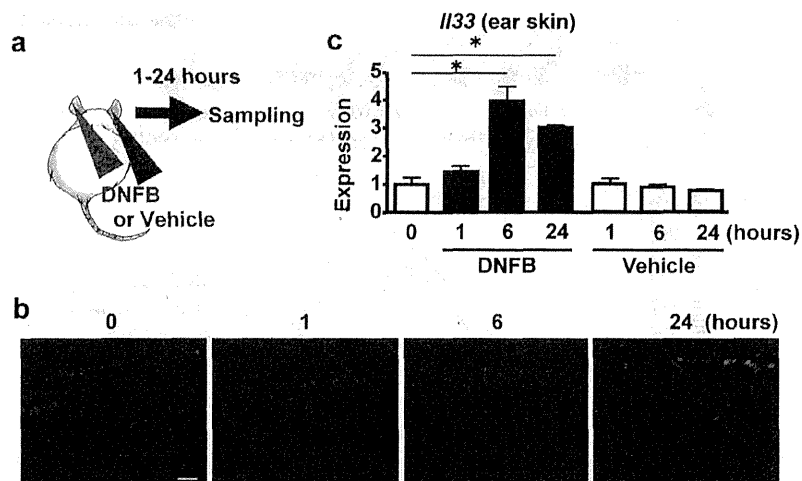
Fig. 2. Expression of IL-33 in the epidermis after DNFB challenge. (a) Naïve WT BALB/c mice were challenged with 20 μl 0.5% DNFB in a 4:1 acetone/olive oil solution on their left ears or with vehicle only on their right ears. (b) Immunofluorescence of IL-33 in the epidermis of WT ear skins. Deparaffinized sections were incubated with an affinity-purified rabbit anti-mouse IL-33 polyclonal antibody [7]. Bound antibodies were visualized with a biotinylated goat anti-rabbit IgG antibody (Vector, Burlingame, CA) and streptavidin-Alexa-594 (Invitrogen, Carlsbad, CA). After mounting with Prolong GOLD Antifade with DAPI (Life Technologies, Gaithersburg, MD), fluorescent images were recorded using a confocal laser-scanning microscope LSM510 (Carl Zeiss, Thornwood, NY). Intense staining of IL-33 is evident in nuclei of the epidermis. Bar, 50 μm. Representative images of 3 independent experiments are shown. (c) Expression of the Il33 gene in the DNFB-treated ear skin. Total RNAs of mouse ears were prepared using an RNeasy Fibrous Tissue Kit (Qiagen, Hilden, Germany). For quantitative real-time PCR, a TaqMan® RNA-to-Ct Kit (Applied Biosystems, Foster City, CA) was used; the product number of the TaqMan® probe for Il33 was Mm00505403_m1. Each bar shows the expression of the Il33 gene in DNFB-treated or vehicle-treated mouse ears (1 h, 6 h, and 24 h) relative to non-treated mice (0 h). Data are expressed as means ± SEM ($n = 4$) and representative data of two independent experiments are shown. $*P < 0.05$ (Dunn's multiple comparison test).

References

[1] Kondo Y, Yoshimoto T, Yasuda K, Futatsugi-Yumikura S, Morimoto M, Hayashi N, et al. Administration of IL-33 induces airway hyperresponsiveness and goblet cell hyperplasia in the lungs in the absence of adaptive immune system. Int Immunol 2008;20:791–800.
[2] Yasuda K, Muto T, Kawagoe T, Matsumoto M, Sasaki Y, Matsushita K, et al. Contribution of IL-33-activated type II innate lymphoid cells to pulmonary eosinophilia in intestinal nematode-infected mice. Proc Natl Acad Sci U S A 2012;109:3451–6.
[3] Haenuki Y, Matsushita K, Futatsugi-Yumikura S, Ishii KJ, Kawagoe T, Imoto Y, et al. A critical role of IL-33 in experimental allergic rhinitis. J Allergy Clin Immunol 2012;130:184–94. e11.
[4] Imai Y, Yasuda K, Sakaguchi Y, Haneda T, Mizutani H, Yoshimoto T, et al. Skin-specific expression of IL-33 activates group 2 innate lymphoid cells and elicits atopic dermatitis-like inflammation in mice. Proc Natl Acad Sci U S A 2013; 110:13921–26.
[5] Natsuaki M, Yano N, Yamaya K, Kitano Y. Immediate contact hypersensitivity induced by repeated hapten challenge in mice. Contact Dermatitis 2000;43:267–72.
[6] Oboki K, Ohno T, Kajiwara N, Arae K, Morita H, Ishii A, et al. IL-33 is a crucial amplifier of innate rather than acquired immunity. Proc Natl Acad Sci U S A 2010;107:18581–86.
[7] Matsuba-Kitamura S, Yoshimoto T, Yasuda K, Futatsugi-Yumikura S, Taki Y, Muto T, et al. Contribution of IL-33 to induction and augmentation of experimental allergic conjunctivitis. Int Immunol 2010;22:479–89.
[8] Hueber AJ, Alves-Filho JC, Asquith DL, Michels C, Millar NL, Reilly JH, et al. IL-33 induces skin inflammation with mast cell and neutrophil activation. Eur J Immunol 2011;41:2229–37.

Yasutomo Imai[a,*], Koubun Yasuda[b], Yoshiko Sakaguchi[a], Shizue Futatsugi-Yumikura[c], Tomohiro Yoshimoto[c], Kenji Nakanishi[b], Kiyofumi Yamanishi[a]

[a]Department of Dermatology, Hyogo College of Medicine, Nishinomiya, Japan; [b]Department of Immunology and Medical Zoology, Hyogo College of Medicine, Nishinomiya, Japan; [c]Laboratory of Allergic Diseases, Institute for Advanced Medical Sciences, Hyogo College of Medicine, Nishinomiya, Japan

*Corresponding author at: Department of Dermatology, Hyogo College of Medicine, 1-1, Mukogawa-cho, Nishinomiya, Hyogo 663-8501, Japan. Tel.: +81 798 45 6653; fax: +81 798 45 6651
E-mail address: imai-yas@hyo-med.ac.jp (Y. Imai).

Pathogenic T$_h$2-type follicular helper T cells contribute to the development of lupus in *Fas*-deficient mice

Shizue Futatsugi-Yumikura[1,2,*], Kazufumi Matsushita[1,*], Ayumi Fukuoka[1,3], Suzuka Takahashi[3,4], Nayu Yamamoto[3], Shin Yonehara[3], Kenji Nakanishi[2] and Tomohiro Yoshimoto[1]

[1]Laboratory of Allergic Diseases, Institute for Advanced Medical Sciences, Hyogo College of Medicine, Nishinomiya, Hyogo 663-8501, Japan
[2]Department of Immunology and Medical Zoology, Hyogo College of Medicine, Nishinomiya, Hyogo 663-8501, Japan
[3]Laboratory of Molecular and Cellular Biology, Graduate School of Biostudies, Kyoto University, Kyoto 606-8501, Japan
[4]Present address: Institute for Genome Research, Tokushima University, Tokushima 770-8503, Japan

Correspondence to: T. Yoshimoto; E-mail: tomo@hyo-med.ac.jp

*These authors contributed equally to this study.

Abstract

Fas mutant mice are well recognized as autoimmune mouse models, which develop symptoms similar to human systemic lupus erythematosus. Although disease severity in Fas mutant mice is greatly affected by the genetic background, the mechanisms affecting pathological heterogeneity among different strains of Fas mutant mice are poorly understood. In this study, we examined the phenotypic differences between Fas-deficient (Fas$^{-/-}$) mice on the BALB/c and C57BL/6 backgrounds to gain insight into the etiological and pathological heterogeneity of monogenic autoimmune diseases. Fas$^{-/-}$ mice on the BALB/c background (BALB/c-Fas$^{-/-}$) developed more severe autoimmune disease with high serum auto-antibodies and renal disease compared with those on the C57BL/6 background (C57BL/6-Fas$^{-/-}$). Splenic B cells were highly activated, and germinal center formation was enhanced in BALB/c-Fas$^{-/-}$ but not in C57BL/6-Fas$^{-/-}$ mice. Follicular helper T (Tfh) cells were equally abundant in the spleens from both strains of Fas$^{-/-}$ mice. However, Tfh cells from BALB/c-Fas$^{-/-}$ mice produced much higher amounts of B-cell-activating cytokines, including IL-4 and IL-10, a phenotype reminiscent of T$_h$2-type Tfh cells described in human studies. Our results revealed a qualitative difference in Tfh cells between the two strains of Fas$^{-/-}$ mice. We propose that the pathogenic T$_h$2-type Tfh cells in BALB/c-Fas$^{-/-}$ mice contribute to the excessive activation of B cells, resulting in high serum immunoglobulin levels and the severe lupus phenotype, which may account for the differential outcomes of human monogenic autoimmune diseases.

Keywords: auto-antibody, CD95, germinal center, IL-4, T$_h$2-type follicular helper T cell

Introduction

The cell surface death receptor, Fas (CD95), is essential for maintaining immune homeostasis and preventing autoimmunity by triggering cellular apoptosis. Studies using spontaneously mutant mouse strains carrying a homozygous defect in *Fas* or *Fas ligand* (*Fasl*) (*Fas*$^{lpr/lpr}$ or *Fasl*$^{gld/gld}$) have shown that loss of the Fas-FasL system causes age-dependent onset of systemic lupus erythematosus (SLE)-like autoimmune diseases characterized by lymphadenopathy and splenomegaly accompanied by lymphoproliferation and auto-antibody production (1, 2). It is well recognized that the genetic backgrounds of mutant mouse strains greatly affect their pathology (3–6). For instance, the original established *Fas*$^{lpr/lpr}$ mice

on an MRL background (MRL-*Fas*$^{lpr/lpr}$) developed a more severe phenotype compared with those on C57BL/6, BALB/c, C3H or AKR backgrounds (3, 4). Although the MRL strain is an autoimmune-prone strain, mice with the *Fas*$^{lpr/lpr}$ mutation on other genetic backgrounds also show lymphoproliferation and auto-antibody production in varying degrees (5, 6). These studies with *Fas*$^{lpr/lpr}$ mice in a variety of backgrounds have revealed that a single *Fas* gene mutation is sufficient for inducing lymphoproliferation and auto-antibody production, but the magnitude and resulting gross phenotype, such as life span or renal disease, is largely dependent on the genetic background (3–6).

More recently, genetically engineered *Fas*-null (*Fas$^{-/-}$*) mice on a 129/C57BL/6 congenic background developed a more severe autoimmune phenotype compared with MRL-*Fas$^{lpr/lpr}$* mice, probably due to the complete loss of the Fas molecule in *Fas$^{-/-}$* mice, whereas the *lpr* mutation is a 'leaky' mutation caused by the insertion of an early transposon into the *Fas* locus (7, 8). We previously generated *Fas$^{-/-}$* mice on the BALB/c (BALB/c-*Fas$^{-/-}$*) (9) and C57BL/6 (C57BL/6-*Fas$^{-/-}$*) backgrounds (10). BALB/c-*Fas$^{-/-}$* mice developed a more severe autoimmune phenotype compared with MRL-*Fas$^{lpr/lpr}$* mice (9). Furthermore, BALB/c-*Fas$^{-/-}$* mice manifest a significant increase in serum IgG1 and IgE levels, and allergy-like symptoms characterized by infiltration of eosinophils and neutrophils into the dermal tissue in eyelids (9, 11). Since the allergy-like symptoms have not been reported in other *Fas* mutant strains, it is a unique pathological phenotype in the BALB/c background mice. These previous studies indicate that the genetic background of autoimmune-prone mice can influence the magnitude of pathology and the qualitative outcomes.

Human FAS- or FAS-related molecule-deficient syndrome is known as autoimmune lymphoproliferative syndrome (ALPS). ALPS patients manifest autoimmune symptoms closely resembling those in *Fas$^{lpr/lpr}$* or *Fas$^{gld/gld}$* mice (12). However, as with other autoimmune diseases, wide clinical heterogeneity is observed among ALPS patients (12). In addition to the type of mutation in the same gene or differences in hetero- and homo-zygous genotypes, multiple genetic factors must be involved in the ALPS pathology, as most autoimmune syndromes are recognized as multifactorial diseases (12, 13). Importantly, some ALPS patients manifest eosinophilia and high serum IgE levels (14), analogous to the phenotype observed in BALB/c-*Fas$^{-/-}$* mice (9). Although recent genome-wide association studies revealed several susceptibility genes and loci for autoimmune diseases, the complex relationship of genetic factors and disease pathology has not been fully elucidated. Therefore, further studies on the genetic factors affecting autoimmune syndromes are essential for both a thorough understanding of the etiology and pathology of human autoimmunity, and establishing effective therapies.

A precise comparison of *Fas$^{-/-}$* mice with different genetic backgrounds will provide important information regarding the etiological and pathological heterogeneity of autoimmune diseases. The aim of this study was to investigate the disease exacerbation factors in *Fas$^{-/-}$* mice. We used two different backgrounds of *Fas$^{-/-}$* mice (BALB/c- and C57BL/6-*Fas$^{-/-}$*) and examined differences in their phenotype to gain insight into factors affecting autoimmune disease.

Methods

Mice

Wild-type BALB/c and C57BL/6 mice were purchased from Charles River Laboratories Japan, Inc. (Yokohama, Japan). *Fas$^{-/-}$* mice on the BALB/c and the C57BL/6 backgrounds were generated by back-crossing *Fas$^{-/-}$* mice (7) to the respective wild-type strains for over seven generations (9, 10). Mice were maintained under specific pathogen-free conditions, where they received sterilized food and water *ad libitum*. All experiments were performed in accordance with the guidelines of the Institutional Animal Care Committee of Hyogo College of Medicine.

Antibodies and reagents

mAbs used in this study were specific for mouse B220 (RA3-6B2), CD3ε (145-2C11), CD4 (RM4-5), CD28 (37.51), CD44 (IM7), CD62L (MEL-14), CD138 (281-2), CD278 (RMP1-30), CXCR5 (2G8), GL-7 (GL-7), IgD (11-26C), IgG1 (M1-14D12) and IgM (R6-60.2). These antibodies were purchased from eBioscience (San Diego, CA, USA), Biolegend (San Diego, CA, USA) or BD Biosciences (San Jose, CA, USA). Peanut Agglutinin (PNA) Rhodamine conjugate was purchased from Vector Laboratories (Burlingame, CA, USA).

Flow cytometry

Cell suspensions of spleen were prepared by sieving and gentle pipetting. For surface staining, cells were maintained in the dark at 4°C. Cells were washed in ice-cold staining buffer (1% BSA in PBS), then incubated with each antibody for 15min and washed twice with staining buffer. Data were acquired on a FACSCanto II flow cytometer (BD Biosciences) and analyzed using FlowJo software (version 7.6.1; Tree Star, Inc., Ashland, OR, USA).

Detection of serum immunoglobulins

Mouse serum IgM, IgG1, IgG2a, IgG2b, IgG2c, IgA and IgE levels were measured by ELISA using polyvalent goat anti-mouse IgM, IgG1, IgG2a, IgG2b, IgG2c or IgA antibodies, or rat anti-mouse IgE mAb (23G3) (SouthernBiotech, Birmingham, AL, USA) as capture antibodies and biotin-conjugated polyvalent goat anti-mouse IgG1, IgG2b or IgG2c antibodies (SouthernBiotech) or biotin-conjugated rat anti-mouse IgM (R6-60.2), IgG2a (R1G-15), IgA (C10-1) or IgE (R35-118) mAbs (BD Biosciences) to the relevant specific isotypes as secondary antibodies. The serum auto-antibody levels were determined by ELISA kits for antinuclear antibodies (ANAs) and anti-Ro/SSA antibodies (Diagnostic Automation, Inc., Calabasas, CA, USA) following the manufacturer's instructions. The differential isotypes of ANAs were determined by using antigen-coated plate from ELISA kits for ANAs and secondary antibodies for each isotype of immunoglobulins.

Histological examination

Tissues were fixed in 4% (w/v) paraformaldehyde, embedded in paraffin, sectioned at 4 μm and stained with hematoxylin and eosin (HE) or Periodic acid–Schiff (PAS) stain. For IgG1 and C3 staining, frozen sections of freshly isolated kidney specimens were incubated with FITC-conjugated anti-IgG1 mAb or FITC-conjugated goat anti-mouse C3 antibody (Immunology Consultants Laboratory, Inc., Portland, OR, USA). For germinal center (GC) staining, frozen sections of freshly isolated spleen specimens were incubated with allophycocyanin (APC)-conjugated anti-IgD mAb and PNA rhodamine conjugate, and then mounted with Prolong Antifade Gold with DAPI (Invitrogen, San Diego, CA, USA). The immunostaining of each section was evaluated under

a microscope (Zeiss LSM 510; Carl Zeiss, Oberkochen, Germany). Computer software, Zeiss LSM 510 ver. 3.2 (Carl Zeiss), was used for image processing.

In vitro follicular helper T-cell stimulation

For the preparation of CD4$^+$B220$^-$CD62L$^-$CD44$^+$CXCR5$^+$PD-1$^+$ follicular helper T (Tfh) cells from BALB/c- and C57BL/6-Fas$^{-/-}$ mice, splenocytes were stained with V-500-conjugated anti-CD4, Percp-Cy5.5-conjugated anti-B220, APC-conjugated anti-CD44, PE-conjugated anti-CD62L, FITC-conjugated PD-1, biotin-conjugated CXCR5 and streptavidin-PE-Cy7 and sorted by FACSAria I (BD Biosciences). Tfh cells (2 × 10^5 cells in 200 µl per well in 96-well flat plates) were cultured with immobilized anti-CD3 and anti-CD28 (each at 5 µg ml^{-1} for coating) for 2 days in RPMI-1640 (Sigma, St Louis, MO, USA) supplemented with 10% (v/v) fetal bovine serum, penicillin (100 U ml^{-1}), streptomycin (100 µg ml^{-1}), L-glutamine (2 mM) and β-mercaptoethanol (50 µM). Supernatants were collected, and cytokine production was assessed by using the Bio-Plex™ System (Bio-Rad Laboratories, Inc., Tokyo, Japan).

Detection of cytokines by cytokine multiplex assay

Bio-Plex™ Pro mouse cytokine multiplex assay kits and the Bio-Plex™ 200 System with high-throughput fluidic (Bio-Rad Laboratories, Inc.) were used following the manufacturer's instructions.

Reverse transcription–PCR

Total RNAs from splenic Tfh cells or B cells were prepared using RNeasy MiniKits (Qiagen, Venlo, Netherlands) and cDNA was synthesized using ReverTra Ace (Toyobo, Osaka, Japan). The expression of genes was quantified with TaqMan Gene Expression Assays (Applied Biosystems) and the Thermal cycler dice RT-PCR system (Takara Bio, Inc., Otsu, Japan) according to the manufacturer's instructions. The results were shown as the relative expression standardized with the expression of a gene encoding eukaryotic 18S ribosomal RNA (rRNA). The specific primers and probes used for quantitative reverse transcription–PCR were TaqMan probes for *Il4*, *IL10*, *Il13*, *Il17*, *Il21*, *Ifng*, *Aicda*, *Bcl6*, *Prdm1* and 18S rRNA (Applied Biosystems).

Statistical analysis

Statistical significance was determined by Bonferroni's multiple comparison test or two-tailed Student's *t*-test. *P* values <0.05 were considered statistically significant. All experiments were performed two or three times and representative results are shown.

Results

Hyperimmunoglobulinemia in BALB/c-Fas$^{-/-}$ mice

We previously reported that BALB/c-Fas$^{-/-}$ mice show higher serum IgG1, IgE and auto-antibody levels (ANAs and anti-Ro/SSA antibodies) compared with MRL-Fas$^{lpr/lpr}$ mice (9, 11). However, the *lpr* mutation does not result in the complete loss of Fas, making it difficult to conclude that the BALB/c background causes higher auto-antibody titers. To determine

the impact of Fas null mutation in different backgrounds, we used two immunologically well-characterized mouse strains, BALB/c and C57BL/6 mice, as genetic backgrounds for Fas$^{-/-}$ mice. All immunoglobulins tested were elevated in BALB/c-Fas$^{-/-}$ mice compared with wild-type BALB/c mice. Especially, IgG1, IgG2a, IgA and IgE levels were significantly higher in BALB/c-Fas$^{-/-}$ mice (Fig. 1A). Only IgG2c levels, which are the C57BL/6 counterpart of IgG2a in the BALB/c strain, were significantly higher in C57BL/6-Fas$^{-/-}$ mice compared with wild-type C57BL/6 mice. However, other immunoglobulin isotypes were comparable between C57BL/6-Fas$^{-/-}$ mice and wild-type C57BL/6 mice (Fig. 1A). As we showed previously (9), BALB/c-Fas$^{-/-}$ mice developed high serum ANAs and anti-Ro/SSA antibodies, whereas negligible levels of serum auto-antibodies were detected in C57BL/6-Fas$^{-/-}$ mice (Fig. 1B). Furthermore, we examined the isotypes of ANAs in the sera. As expected, high levels of IgM, IgG1 and IgG2a ANAs were detected in BALB/c-Fas$^{-/-}$ mice (Supplementary Figure S1, available at *International Immunology* Online). These results demonstrated that self-reactive B cells were highly activated and received signals for class switch recombination in BALB/c-Fas$^{-/-}$ mice. BALB/c-Fas$^{-/-}$ mice showed age-dependent auto-antibody production similar to other Fas mutant mouse strains, which was maximal at ~20 weeks of age (Fig. 1B). Thus, we used mice at around 20 weeks old (18–23 weeks old) for the later studies.

Serological examinations indicated that Fas$^{-/-}$ mice on the BALB/c background showed a more severe autoimmune phenotype compared with C57BL/6 background mice in terms of hyperimmunoglobulinemia.

Glomerulonephritis-like symptoms in BALB/c-Fas$^{-/-}$ mice

A characteristic pathology induced by high serum auto-antibody levels is immune complex-mediated renal disease (15). Although auto-antibody production is observed in almost all mouse strains carrying homozygous Fas mutations, pathological features in the kidney differ greatly among them (5, 6). Thus, we examined the histopathology and immunohistochemistry of kidneys from BALB/c- and C57BL/6-Fas$^{-/-}$ mice. Serum IgG1 antibody levels were high in BALB/c-Fas$^{-/-}$ mice (Fig. 1A) and intense glomerular IgG1 deposition was detected in the kidneys. Although IgG1 deposition was also detected in C57BL/6-Fas$^{-/-}$ mice, but not in wild-type mice, the magnitude was much lower than in BALB/c-Fas$^{-/-}$ mice (Fig. 2A). Since levels of complement-fixing antibodies such as IgG2a were high in BALB/c-Fas$^{-/-}$ mice (Fig. 1A), we also examined the deposition of complement component C3, which is an important and a characteristic feature of immune complex-mediated renal diseases (15). Again, BALB/c-Fas$^{-/-}$ mice showed the highest glomerular C3 deposition in the kidneys among the mice investigated (Fig. 2B). In addition, histological examination of the kidneys revealed that PAS-positive matrix was abundant and the epithelia of Bowman's capsule formed a cylindrical structure in the glomeruli in BALB/c-Fas$^{-/-}$ mice. In contrast, little change was observed in the glomeruli of C57BL/6-Fas$^{-/-}$ mice compared with wild-type mice (Fig. 2C). In addition, urinary protein excretion was higher in BALB/c-Fas$^{-/-}$ mice compared with C57BL/6-Fas$^{-/-}$ mice (data not shown). These results clearly
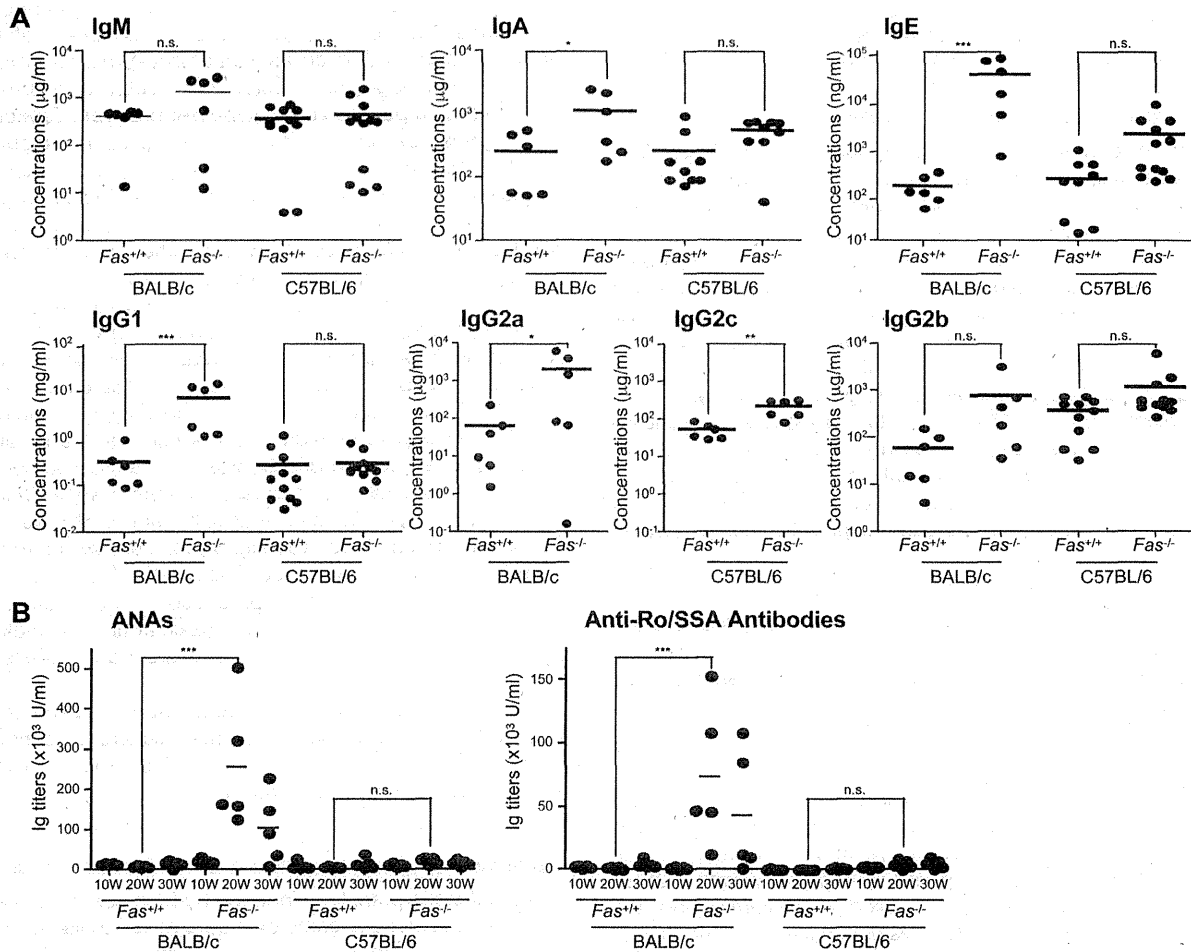
Fig. 1. Hyperimmunoglobulinemia in BALB/c-*Fas$^{-/-}$* mice. (A) Serum immunoglobulin (Ig) concentrations in 20-week-old BALB/c and C57BL/6 wild-type (*Fas$^{+/+}$*) mice, and *Fas*-deficient (*Fas$^{-/-}$*) mice were measured by ELISA (BALB/c-*Fas$^{+/+}$* and BALB/c-*Fas$^{-/-}$*, n = 6; C57BL/6-*Fas$^{+/+}$*, n = 11 and C57BL/6-*Fas$^{-/-}$*, n = 12). (B) Sera were collected from BALB/c and C57BL/6 wild-type (*Fas$^{+/+}$*) mice, and *Fas*-deficient (*Fas$^{-/-}$*) mice at 10, 20 and 30 weeks of age (all n = 5). The levels of ANAs and anti-Ro/SSA antibodies were determined by ELISA. Each symbol represents a single mouse and horizontal lines indicate the mean values. Statistical significance was determined by Bonferroni's multiple comparison test. ***$P < 0.001$, **$P < 0.01$, *$P < 0.05$, n.s., not significant.

indicate that BALB/c-*Fas$^{-/-}$* but not C57BL/6-*Fas$^{-/-}$* mice suffer from immune complex-mediated renal disease histologically resembling glomerulonephritis.

In contrast to auto-antibody production and renal disease, both BALB/c-*Fas$^{-/-}$* and C57BL/6-*Fas$^{-/-}$* mice showed considerable accumulation of unusual CD3$^+$B220$^+$ cells [also referred to as lpr cells or double-negative (DN) T cells] in the spleen, which is a characteristic phenotype in *Fas*- or *Fasl*-deficient mice and ALPS patients (12, 13) (Supplementary Figure S2, available at *International Immunology* Online). In addition, HE staining of tissues indicated strong signs of lymphoinfiltration into tissues including spleen, lung and liver in both strains of *Fas$^{-/-}$* mice (Supplementary Figure S3, available at *International Immunology* Online).

Taken together, BALB/c-*Fas$^{-/-}$* mice developed severe auto-immune symptoms, auto-antibody production and renal disease, which have been well characterized in other *Fas* mutant

strains, with a magnitude higher than for C57BL/6-*Fas$^{-/-}$* mice. However, the exacerbated pathology in BALB/c-*Fas$^{-/-}$* mice was specifically observed for auto-antibody-mediated symptoms, although both *Fas$^{-/-}$* mice showed comparable lymphoproliferative symptoms.

Enhanced B-cell activation and GC formation in BALB/c-Fas$^{-/-}$ mice

Since BALB/c-*Fas$^{-/-}$* mice showed hyperimmunoglobulinemia and auto-antibody production, we next examined B-cell activation status in the spleens. As shown in Fig. 3(A), IgM and IgD DN B cells (gated on CD3$^-$B220$^+$ cells), which indicated class-switched B cells, were significantly more abundant in BALB/c-*Fas$^{-/-}$* mice compared with wild-type mice. C57BL/6-*Fas$^{-/-}$* mice also showed a tendency of increased class-switched B cells, although this was not statistically significant
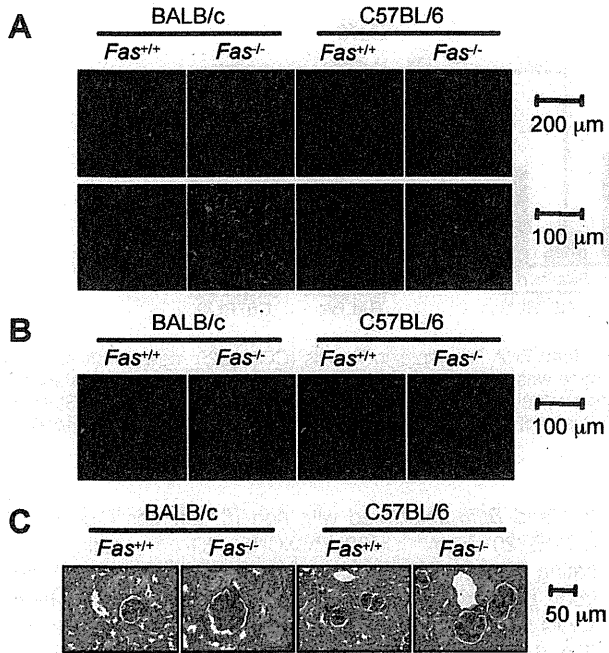
A

BALB/c		C57BL/6	
Fas$^{+/+}$	*Fas$^{-/-}$*	*Fas$^{+/+}$*	*Fas$^{-/-}$*

⊢⊣ 200 μm

⊢⊣ 100 μm

B

BALB/c		C57BL/6	
Fas$^{+/+}$	*Fas$^{-/-}$*	*Fas$^{+/+}$*	*Fas$^{-/-}$*

⊢⊣ 100 μm

C

BALB/c		C57BL/6	
Fas$^{+/+}$	*Fas$^{-/-}$*	*Fas$^{+/+}$*	*Fas$^{-/-}$*

⊢⊣ 50 μm

Fig. 2. Glomerulonephritis-like kidney failure in Balb/c-Fas$^{-/-}$ mice. (A and B) Kidney sections from 20-week-old BALB/c and C57BL/6 wild-type (*Fas$^{+/+}$*) mice, and Fas-deficient (*Fas$^{-/-}$*) mice were stained with FITC-labeled anti-mouse IgG1 mAb (A) or FITC-labeled anti-mouse C3 mAb (B). (C) The same kidney sections were stained with PAS. Data are representative of a single experiment with a total of three mice per genotype.

compared with wild-type mice, and a lower magnitude than in BALB/c-Fas$^{-/-}$ mice. The frequencies of immunoglobulin class-switched B cells within splenic B cells in BALB/c- and C57BL/6-Fas$^{-/-}$ mice were ~17 and 7.5%, respectively (Fig. 3A). Most IgM$^-$IgD$^-$ B cells in BALB/c-Fas$^{-/-}$, but not in C57BL/6-Fas$^{-/-}$ mice, expressed IgG1 on their surface, indicating an accumulation of IgG1$^+$ memory B cells in BALB/c-Fas$^{-/-}$ mice (Fig. 3B). The GC is an important immunological site for B cells to undergo immunoglobulin class switching and antibody affinity maturation (16). Thus, we investigated the difference in GC formation in the spleens of the Fas$^{-/-}$ mice. FACS analysis revealed that ~5% of B cells in BALB/c-Fas$^{-/-}$ mice were PNA$^+$ and GL-7+ GC B cells, whereas GC B cells were almost undetectable in wild-type controls (Fig. 3C). Immunohistochemical examination of spleens from BALB/c-Fas$^{-/-}$ mice showed the presence of PNA$^+$ cells inside the B-cell follicle, clearly indicating GC formation (Fig. 3D). In contrast, PNA$^+$GL-7$^+$ GC B cells were comparable between C57BL/6-Fas$^{-/-}$ mice and wild-type controls and little or no GC formation was detectable in C57BL/6-Fas$^{-/-}$ mouse spleens (Fig. 3C and D). Again, B-cell hyperactivation was evident in BALB/c-Fas$^{-/-}$, but not in C57BL/6-Fas$^{-/-}$ mice.

Next, we examined mRNA expression in splenic B cells. Compared with wild-type B cells, BALB/c-Fas$^{-/-}$ B cells expressed >35-fold higher levels of mRNA for activation-induced cytidine deaminase (AID), encoded by *Aicda*, which is essential for induction of B-cell class switching and antibody affinity maturation (17) (Fig. 4). In C57BL/6-Fas$^{-/-}$ mice, *Aicda* expression in B cells was comparable to wild-type cells. The expression of Blimp-1, encoded by *Prdm1*, which is required for B cells to differentiate into plasma cells (18),
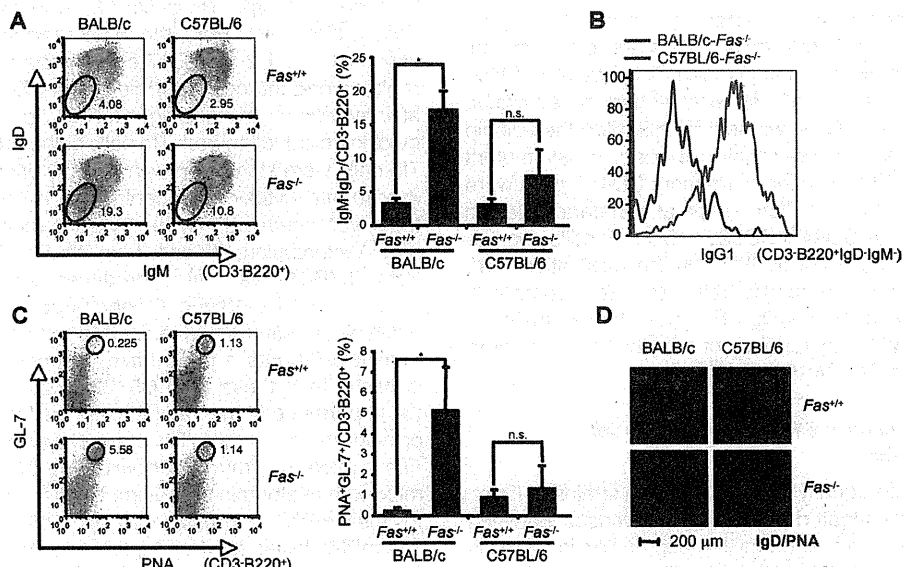

Fig. 3. Enhanced class switching and germinal center formation in Balb/c-Fas$^{-/-}$ mice. (A–C) Flow cytometric analysis was performed on splenocytes from 20-week-old BALB/c and C57BL/6 wild-type (*Fas$^{+/+}$*) mice, and Fas-deficient (*Fas$^{-/-}$*) mice. Expression of IgM and IgD (A), PNA and GL-7 (C) in splenic B cells (CD3$^-$B220$^+$ cells), and of IgG1 in CD3$^-$B220$^+$IgM$^-$IgD$^-$ cells (B) were examined. The representative flow cytometry plots and the quantified graphs (the mean value ± SD from three mice) are indicated. Statistical significance was determined by Student's t-test. *P < 0.05, n.s., not significant. (D) Frozen sections of freshly isolated spleen specimens were stained with APC-conjugated anti-IgD mAb and rhodamine-conjugated PNA. The representative images of a total of three independent experiments are shown.
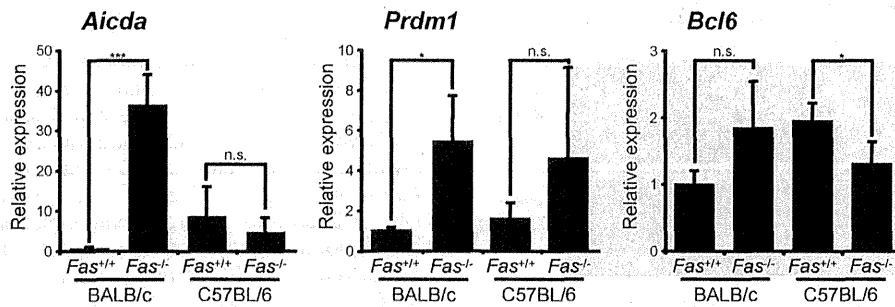
Fig. 4. Spontaneous activation of splenic B cells in BALB/c-*Fas*$^{-/-}$ mice. Total RNA from splenic B cells (CD3$^-$B220$^+$ cells) in 20-week-old BALB/c and C57BL/6 wild-type mice (*Fas*$^{+/+}$), and *Fas*-deficient (*Fas*$^{-/-}$) mice was extracted and subjected to quantitative reverse transcription–PCR for the expression of *Aicda*, *Prdm1*, *Bcl6* and 18S rRNA. The mean value ± SD from three mice in each genotype is shown. Statistical significance was determined by Student's *t*-test. ***P < 0.001, *P < 0.05, n.s., not significant. The representative images of two independent experiments are shown.

was also up-regulated in BALB/c-*Fas*$^{-/-}$ mice. B cells from C57BL/6-*Fas*$^{-/-}$ mice expressed comparably high levels of *Prdm1*, even though this was not statistically significant when compared with wild-type controls (Fig. 4). A transcriptional repressor in B cells, Bcl-6 (18), encoded by *Bcl6*, was not augmented in *Fas*$^{-/-}$ B cells of both strains (Fig. 4).

These results clearly indicated that B cells were highly activated, and GC formation and immunoglobulin class switching were enhanced in BALB/c-*Fas*$^{-/-}$ mice, to which the hyperimmunoglobulinemia was attributable.

Comparable frequency of Tfh cells between BALB/c- and C57BL/6-Fas$^{-/-}$ mice

Tfh cells are a distinct subset of CD4$^+$ helper T cells that regulate the development of antigen-specific humoral immunity by providing essential help for B cells in GCs and play a critical role in the development of autoimmune diseases (16). Since BALB/c-*Fas*$^{-/-}$ mouse B cells showed enhanced activation and class switching in GCs, we next investigated the splenic Tfh cell population. As previously reported, in *lpr* mutant strains, CD44^{high}CD62L^{low} effector/memory CD4$^+$ T cells were abundant in both strains of *Fas*$^{-/-}$ mice at comparable levels (Fig. 5A). Within the CD44^{high}CD62L^{low} CD4$^+$ T cells, we further investigated the CXCR5^{high}PD-1^{high} Tfh population (16). Again, Tfh cells were abundant in both *Fas*$^{-/-}$ mice compared with their wild-type controls (Fig. 5B). Thus, the expansion of Tfh cell differentiation alone does not explain the augmented B-cell activation in BALB/c-*Fas*$^{-/-}$ mice.

Qualitative differences in Tfh cells in BALB/c- and C57BL/6-Fas$^{-/-}$ mice

Since Tfh cells were equally abundant in both strains of *Fas*$^{-/-}$ mice, we next investigated qualitative differences between the populations. We examined mRNA expression in Tfh cells (CD4$^+$B220$^-$CD44^{high}CD62L^{low}CXCR5^{high}PD-1^{high} cells) freshly isolated from *Fas*$^{-/-}$ mice. Both *Fas*$^{-/-}$ mouse-derived Tfh cells expressed comparable levels of *ll21*, a characteristic cytokine of Tfh cells and essential for B-cell activation in GCs (16), and *Bcl6*, a characteristic and essential transcription factor for Tfh cell development (16). Of note, Tfh cells from both genetic backgrounds expressed higher levels of

ll21 and *Bcl6* compared with non-Tfh effector T cells (Teff; CD4$^+$B220$^-$CD44^{high}CD62L^{low}CXCR5^{low}PD-1^{low} cells), indicating Tfh cells were authentic Tfh cells. However, Tfh cells from BALB/c-*Fas*$^{-/-}$ mice expressed significantly higher levels of *ll4* and *ll10* than those from C57BL/6-*Fas*$^{-/-}$ mice (Fig. 6A). These cytokines have essential roles in B-cell activation, survival and antibody production (19–22). In addition, high *ll13* expression was detected in Tfh cells from BALB/c-*Fas*$^{-/-}$ mice (Supplementary Figure S4A, available at *International Immunology* Online). In contrast, *ll17* and *Ifng* expression were not increased in Tfh cells from BALB/c-*Fas*$^{-/-}$ mice compared with Tfh cells from C57BL/6-*Fas*$^{-/-}$ mice (Supplementary Figure S4A, available at *International Immunology* Online). This cytokine profile is similar to that of human T_h2-type Tfh cells (18). The expression levels of *Tbx21*, *Gata3* and *Rorc*, the master regulator genes for conventional T_h1, T_h2 and T_h17 cells, respectively, were comparable among the cells (Supplementary Figure S4A, available at *International Immunology* Online). To examine further the cytokine production from Tfh cells at the protein level, purified Tfh cells were stimulated with anti-CD3/anti-CD28 antibodies *in vitro* and cytokine concentrations in the culture supernatants were measured by the cytokine multiplex assay. As for mRNA expression, Tfh cells from BALB/c-*Fas*$^{-/-}$ mice, but not from C57BL/6-*Fas*$^{-/-}$ mice, produced substantial amounts of IL-4, IL-10 and IL-13 (Fig. 6B and Supplementary Figure S4B, available at *International Immunology* Online). Thus, Tfh cells from BALB/c-*Fas*$^{-/-}$ mice have a stronger B-cell-activating capacity than those from C57BL/6-*Fas*$^{-/-}$ mice. To examine the importance of the *Fas*-deficient environment in the development of the unique Tfh phenotype observed in BALB/c-*Fas*$^{-/-}$ mice, we immunized wild-type BALB/c and C57/BL6 mice with ovalbumin and alum, and Tfh cells were examined for their mRNA expression 10 days after the immunization. The mRNA levels for *ll4*, *ll10*, *ll21* and *Bcl6* were comparable between the Tfh cells from wild-type BALB/c and C57/BL6 mice (data not shown). Thus, T_h2-type Tfh cells are uniquely generated in BALB/c-*Fas*$^{-/-}$ mice, and the population may be prone to be eliminated by Fas-mediated apoptosis in a normal course of the immune response in wild-type mice.

Taken together, our results indicate that although both BALB/c-*Fas*$^{-/-}$ and C57BL/6-*Fas*$^{-/-}$ mice have a comparable
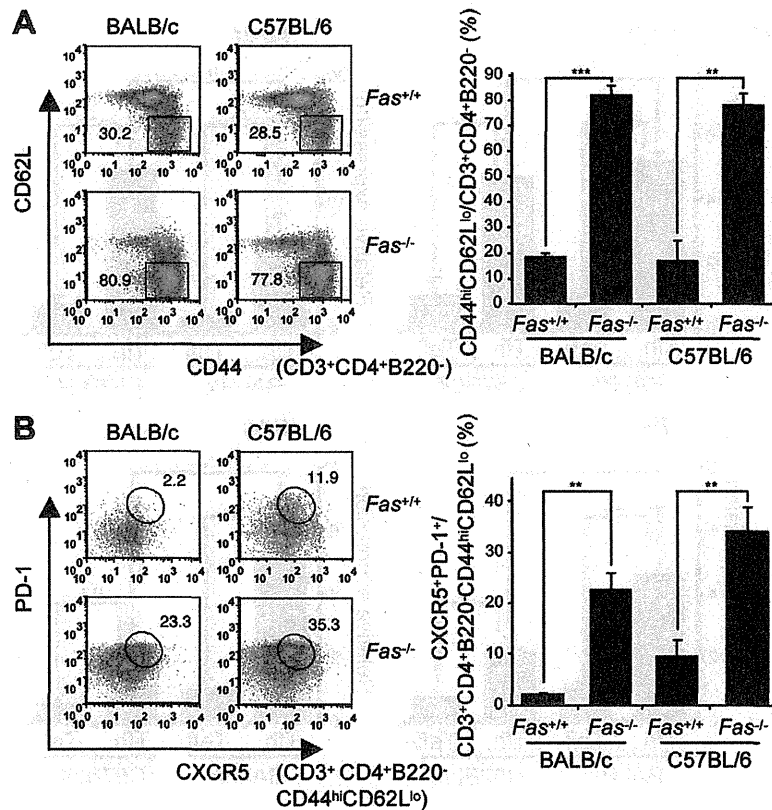
Fig. 5. Tfh cells are comparably abundant in BALB/c- and C57BL/6-*Fas*^{-/-} mice. Flow cytometric analysis was performed on splenocytes from 20-week-old BALB/c and C57BL/6 wild-type (*Fas*^{+/+}) mice, and *Fas*-deficient (*Fas*^{-/-}) mice. Expression of CD44 and CD62L in splenic CD4⁺ T cells (CD3⁺CD4⁺B220⁻ cells) (A), and CXCR5 and PD-1 in splenic effector/memory T cells (CD4⁺B220⁻CD44^{high}CD62L^{low} cells) (B) were determined. The representative flow cytometry plots and the quantified graphs (the mean value ± SD from three mice) are indicated. Statistical significance was determined by Student's *t*-test. ***P < 0.001, **P < 0.01. The representative images of three independent experiments are shown.

frequency of Tfh cells, they are qualitatively different, and that BALB/c-*Fas*^{-/-} mouse-derived Tfh cells produce higher amounts of B-cell-activating cytokines. We propose that IL-4 and IL-10 are the candidate cytokines that may contribute to enhanced B-cell activation and high immunoglobulin production in BALB/c-*Fas*^{-/-} mice. Furthermore, the phenotype of Tfh cells in BALB/c-*Fas*^{-/-} mice is reminiscent of T_h2-type Tfh cells described in human studies (18).

Discussion

In this study, we examined the phenotypic differences of *Fas*^{-/-} mice with BALB/c and C57BL/6 genetic backgrounds. BALB/c-*Fas*^{-/-} mice developed more severe autoimmune symptoms including hyperimmunoglobulinemia and renal disease, whereas no difference was observed in tissue lymphoinfiltration between these strains. Splenic B cells in BALB/c-*Fas*^{-/-} mice were strongly activated, expressed high levels of AID and differentiated into class-switched memory B cells. The GC is an essential immunological site for B-cell class switching and antibody affinity maturation, and BALB/c-*Fas*^{-/-} mice developed GC formation in the spleen. In contrast, C57BL/6-*Fas*^{-/-} mice showed negligible auto-antibody

production and B-cell activation. These results indicated that antibody production-mediated symptoms observed in *Fas*^{-/-} mice were highly exacerbated in mice with a BALB/c background. It is well recognized that the disease phenotype of *Fas* mutant mice is greatly affected by the genetic background. Auto-antibody production and renal disease in *Fas*^{lpr/lpr} mice with MRL, C57BL/6, BALB/c, C3H or AKR backgrounds have been investigated (1–6). However, the mechanisms involved in the differences have not been fully investigated. In this study, we examined the potential cause of pathological heterogeneity of *Fas*^{-/-} mice on different genetic backgrounds. We showed that Tfh cells from BALB/c-*Fas*^{-/-} mice have a different cytokine profile compared with Tfh cells from C57BL/6-*Fas*^{-/-} mice, by producing more IL-4 and IL-10 than those from C57BL/6-*Fas*^{-/-} mice.

The accumulation of Tfh cells in *Fas* mutant mice was also reported in previous studies using MRL-*Fas*^{lpr/lpr}, C57BL/6-*Fas*^{-/-} or their congenic strains (23, 24). The initiation of Tfh cells and GC B-cell-mediated responses is not fully understood. Both Tfh cells and GC B cells may be essential for the development of each other (16). Regarding the disease symptoms in *Fas*-deficient mice, conditional deletion of the *Fas* gene specifically in B cells or GC B cells reproduces
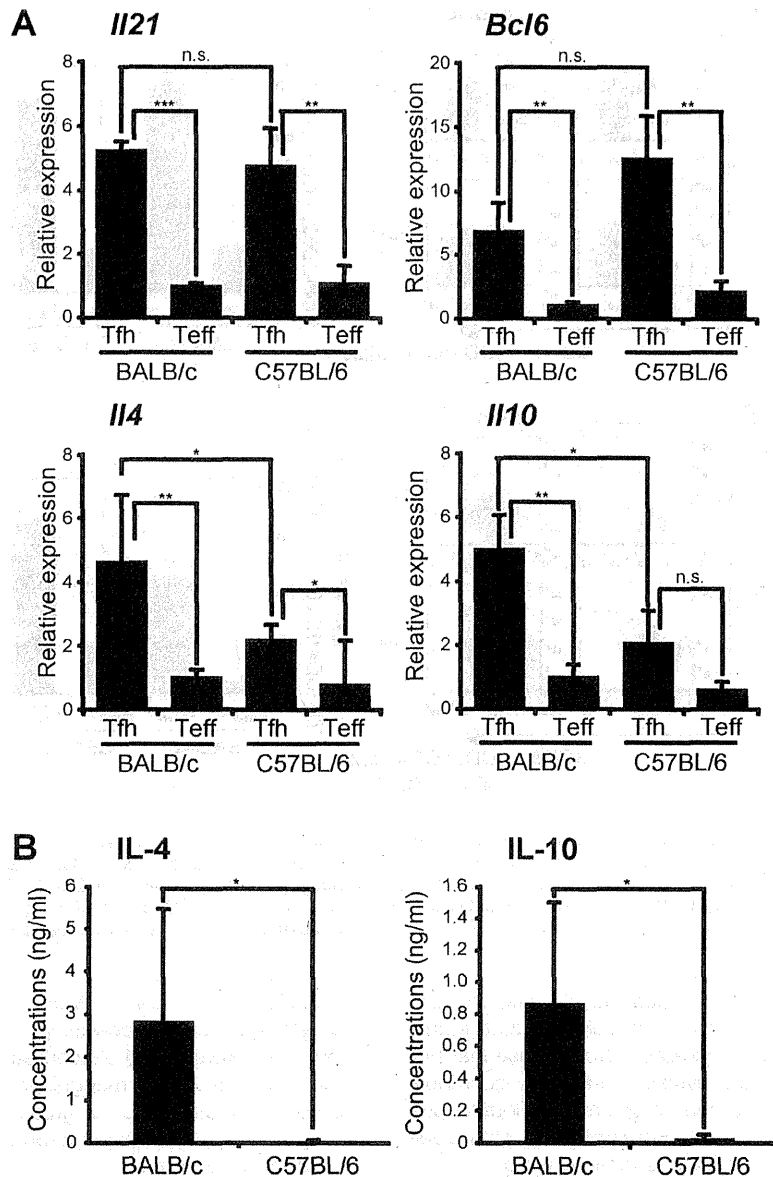
Fig. 6. Augmented production of B-cell-activating cytokines from Tfh cells in Balb/c-*Fas*$^{-/-}$ mice. (A) Tfh cells (CD4⁺B220⁻CD44^{high}CD62L^{low} CXCR5^{high}PD-1^{high} cells) and effector T cells (Teff; CD4⁺B220⁻CD44^{high}CD62L^{low}CXCR5^{low}PD-1^{low} cells) from 20-week-old BALB/c and C57BL/6 *Fas*-deficient (*Fas*$^{-/-}$) mice were sorted, total RNAs extracted and subjected to quantitative reverse transcription–PCR for the expression of *Il21*, *Bcl6*, *Il4*, *Il10* and 18S rRNA. (B) Tfh cells from 20-week-old BALB/c and C57BL/6 *Fas*-deficient (*Fas*$^{-/-}$) mice were sorted and stimulated with anti-CD3 and anti-CD28 (each 5 µg ml⁻¹) for 48 h. The cytokine concentrations in the culture supernatants were determined by the Bio-Plex cytokine multiplex assay. The mean value ± SD from three mice in each genotype is shown. Statistical significance was determined by Student's *t*-test. ***P < 0.001, **P < 0.01, *P < 0.05, n.s., not significant. The representative images of two independent experiments are shown.

the disease phenotype observed in conventional *Fas* mutant mice, suggesting that B cells, especially GC B cells, have an essential role in initiating the pathology of *Fas* mutant mice, as Fas is highly expressed on GC B cells (23). Even though B-cell-specific *Fas*-deficient mice develop autoimmunity and have early mortality, the removal of T cells or deletion of CD28 in these mice totally restores the phenotype including B-cell activation (23). In addition, deletion of inducible costimulator (ICOS), which is highly expressed on Tfh cells and plays a critical role in GC B-cell activation (16), in MRL-*Fas*$^{lpr/lpr}$ mice significantly reduced auto-antibody production (25, 26). These studies suggest that although activated B cells play an essential role in initiating disease, interactions between B and T cells, especially Tfh cells in GCs, are important for the progression of antibody production and the pathology. Indeed, we previously showed that splenic B cells

from BALB/c-Fas$^{-/-}$ and wild-type mice produced comparable levels of IgG1 and IgE in response to IL-4 and anti-CD40 antibody stimulation *in vitro* (11). This indicates that B-cell-intrinsic abnormalities alone cannot explain the hyperimmunoglobulinemia observed in BALB/c-Fas$^{-/-}$ mice.

Among the cytokines produced by Tfh cells, IL-21 is characteristic and important for GC B-cell survival and differentiation (16, 27). However, even though *Il21r$^{-/-}$* mice show some humoral immunity defects, they are still capable of developing GC responses (28). Thus, other Tfh cell cytokines must be essential for activating GC B cells. IL-4 may be one of these cytokines, since IL-4 and IL-21R double-deficient mice show pan-hypogammaglobulinemia indicating cooperative roles of the two cytokines (29). IL-4 is well recognized as an indispensable cytokine for B-cell class switching to IgG1 and IgE, of which BALB/c-Fas$^{-/-}$ mice produce large amounts. In addition, accumulating evidence suggests that IL-4 produced by Tfh cells, rather than by T$_h$2 cells, is important for controlling humoral immunity (16, 30–32). IL-10 is another Tfh cytokine (33), which can enhance B-cell antibody production (18). Although IL-10 is considered an anti-inflammatory cytokine that is essential for preventing autoimmunity, IL-10 also has a B-cell-activating capacity (21, 22) and some reports have demonstrated a pathological role for IL-10 in auto-antibody production (34, 35). Thus, IL-10 could also be a predisposing factor for autoimmunity in some disease settings. Taken together, we propose that IL-4 and IL-10 produced by Tfh cells are the likely causes of high GC formation and the severe autoimmune phenotype in BALB/c-Fas$^{-/-}$ mice.

Tfh cells are considered a heterogenic population, which can be further divided into several cell types depending on their cytokine, chemokine or chemokine receptor profiles. Although Tfh cells can produce the T$_h$1 cytokine IFN-γ (36), T$_h$2 cytokine IL-4 (19, 20, 30), or T$_h$17 cytokine IL-17 (37) in certain conditions, the presence of specialized T$_h$1-, T$_h$2- or T$_h$17-type Tfh cells is still controversial (16). However, Morita *et al.* (18) clearly showed that circulating human Tfh cells can be classified into the three subtypes, T$_h$1, T$_h$2 or T$_h$17 type depending on their unique cytokine and chemokine receptor profiles characteristic for conventional T$_h$1, T$_h$2 and T$_h$17 cells, and which differentially help B-cell antibody production. The high IL-4, as well as IL-13, production of Tfh cells from BALB/c-Fas$^{-/-}$ mice suggests they are similar to human T$_h$2-type Tfh cells. This similarity is also seen in their B-cell-helping capacity. BALB/c-Fas$^{-/-}$ mice showed high IgG1, IgG2a and IgE levels in the sera, and human T$_h$2-type Tfh cells preferentially help B cells to produce IgG and IgE antibodies (18). Interestingly, Morita *et al.* (18) also showed that T$_h$2- and T$_h$17-type Tfh cells are more pathogenic than the T$_h$1 type, and skewing of Tfh cells toward T$_h$2 and T$_h$17 types correlates with disease activity in an autoimmune disease, juvenile dermatomyositis. Furthermore, T$_h$2-type Tfh cells have been reported in mice, where IL-4-producing Tfh cells contribute to immunity against helminthic infection by promoting IgE production (19, 20, 30). These reports support our hypothesis that the pathological heterogeneity of the autoimmune phenotype between BALB/c-Fas$^{-/-}$ and C57BL/6-Fas$^{-/-}$ mice is ascribed to their different Tfh cell populations. The accumulation of T$_h$2-type Tfh cells also

explains the unique allergy-like phenotype of BALB/c-Fas$^{-/-}$ mice. We recently identified a novel innate cell population, Fas-expressing natural helper (F-NH) cells, which are abundant in BALB/c-Fas$^{-/-}$ mice and enhance B-cell IgG1 and IgE production in the presence of IL-4 (11). F-NH cells may also enhance IgG1 and IgE production *in vivo*, although the source of IL-4 was unclear (11). The IL-4-producing Tfh cells and F-NH cells may cooperate to augment serum IgG1 and IgE levels and exacerbate the allergy-like phenotype, which is uniquely observed in BALB/c-Fas$^{-/-}$ mice (9).

The human FAS or FAS-related molecule deficiency, ALPS, is characterized by lymphadenopathy, splenomegaly and hypergammaglobulinemia, which are also observed in *Fas* mutant mice (12, 13). Similar to *Fas* mutant mouse models, disease severity differs among patients and, more importantly, some, but not all, ALPS patients manifest eosinophilia and increased serum IgE levels (14). ALPS patients with eosinophilia show a higher mortality rate than those without eosinophilia (14). Although the etiology of eosinophilic ALPS is unexplained, our results may aid our understanding. Disease heterogeneity might be explained by the accumulation of 'pathogenic' Tfh cells. In addition to ALPS, several human diseases, especially auto-antibody-mediated diseases, such as SLE or rheumatoid arthritis, can be caused by the dysregulation of Tfh cells (38). It was reported that serum concentrations of IgE and anti-dsDNA antibodies were associated with disease severity in SLE patients (39, 40). Our results may also provide an important bridge between Tfh phenotype and disease heterogeneity among patients suffering from auto-antibody-mediated diseases.

In addition to *Fas* mutant mice, several gene-targeted mice have been back-crossed onto both the BALB/c and the C57BL/6 background. In some cases, the differential genetic backgrounds have a huge impact on their phenotype. The BALB/c background is not as autoimmune prone compared with the C57BL/6 background. For instance, *Ship1$^{-/-}$* mice show a more severe autoimmune phenotype such as auto-antibody production and glomerulonephritis on the C57BL/6 background compared with the BALB/c background (41). In addition, C57BL/6-*Fcgr2b$^{-/-}$* but not BALB/c-*Fcgr2b$^{-/-}$* mice develop severe autoimmune disease (42). The complex combination of the presence of predisposing factors and absence of protecting factors may explain disease susceptibility and exacerbation in different strains. However, as none of these studies documented direct target genes affecting the phenotype, it remains unclear which genes or loci actually influence the different phenotype between BALB/c- and C57BL/6-*Fas$^{-/-}$* mice. Future studies using gene mapping may uncover the real target(s) of disease exacerbation or protection due to background genotype.

In summary, we showed that BALB/c- and C57BL/6-*Fas$^{-/-}$* mice develop a substantially different phenotype in their disease severity. The accumulation of qualitatively different Tfh cell populations may in part explain the aggressive phenotype of BALB/c-*Fas$^{-/-}$* mice. C57BL/6-*Fas$^{-/-}$* mice, in which Tfh cells also accumulate, show a much milder phenotype. Thus, we hypothesize that 'pathogenic' T$_h$2-type Tfh cells or their cytokines are attractive candidate therapeutic targets in antibody production-mediated autoimmune diseases.

Supplementary data

Supplementary data are available at *International Immunology Online.*

Funding

Acknowledgements

Conflict of Interest statement: The authors have no financial conflicts of interest.

References

1 Strasser, A., Jost, P. J. and Nagata, S. 2009. The many roles of FAS receptor signaling in the immune system. *Immunity* 30:180.
2 Yonehara, S. 2002. Death receptor Fas and autoimmune disease: from the original generation to therapeutic application of agonistic anti-Fas monoclonal antibody. *Cytokine Growth Factor Rev.* 13:393.
3 Warren, R. W., Caster, S. A., Roths, J. B., Murphy, E. D. and Pisetsky, D. S. 1984. The influence of the lpr gene on B cell activation: differential antibody expression in lpr congenic mouse strains. *Clin. Immunol. Immunopathol.* 31:65.
4 Fields, M. L., Sokol, C. L., Eaton-Bassiri, A., Seo, S., Madaio, M. P. and Erikson, J. 2001. Fas/Fas ligand deficiency results in altered localization of anti-double-stranded DNA B cells and dendritic cells. *J. Immunol.* 167:2370.
5 Izui, S., Kelley, V. E., Masuda, K., Yoshida, H., Roths, J. B. and Murphy, E. D. 1984. Induction of various autoantibodies by mutant gene lpr in several strains of mice. *J. Immunol.* 133:227.
6 Kelley, V. E. and Roths, J. B. 1985. Interaction of mutant lpr gene with background strain influences renal disease. *Clin. Immunol. Immunopathol.* 37:220.
7 Senju, S., Negishi, I., Motoyama, N. *et al.* 1996. Functional significance of the Fas molecule in naive lymphocytes. *Int. Immunol.* 8:423.
8 Adachi, M., Suematsu, S., Suda, T. *et al.* 1996. Enhanced and accelerated lymphoproliferation in Fas-null mice. *Proc. Natl Acad. Sci. USA* 93:2131.
9 Takahashi, S., Futatsugi-Yumikura, S., Fukuoka, A., Yoshimoto, T., Nakanishi, K. and Yonehara, S. 2013. Fas deficiency in mice with the Balb/c background induces blepharitis with allergic inflammation and hyper-IgE production in conjunction with severe autoimmune disease. *Int. Immunol.* 25:287.
10 Yajima, N., Sakamaki, K. and Yonehara, S. 2004. Age-related thymic involution is mediated by Fas on thymic epithelial cells. *Int. Immunol.* 16:1027.
11 Fukuoka, A., Futatsugi-Yumikura, S., Takahashi, S. *et al.* 2013. Identification of a novel type 2 innate immunocyte with the ability to enhance IgE production. *Int. Immunol.* 25:373.
12 Cheng, M. H. and Anderson, M. S. 2012. Monogenic autoimmunity. *Annu. Rev. Immunol.* 30:393.
13 Goodnow, C. C. 2007. Multistep pathogenesis of autoimmune disease. *Cell* 130:25.
14 Kim, Y. J., Dale, J. K., Noel, P. *et al.* 2007. Eosinophilia is associated with a higher mortality rate among patients with autoimmune lymphoproliferative syndrome. *Am. J. Hematol.* 82:615.
15 Nowling, T. K. and Gilkeson, G. S. 2011. Mechanisms of tissue injury in lupus nephritis. *Arthritis Res. Ther.* 13:250.
16 Ma, C. S., Deenick, E. K., Batten, M. and Tangye, S. G. 2012. The origins, function, and regulation of T follicular helper cells. *J. Exp. Med.* 209:1241.
17 Muramatsu, M., Kinoshita, K., Fagarasan, S., Yamada, S., Shinkai, Y. and Honjo, T. 2000. Class switch recombination and hypermutation require activation-induced cytidine deaminase (AID), a potential RNA editing enzyme. *Cell* 102:553.
18 Morita, R., Schmitt, N., Bentebibel, S. E. *et al.* 2011. Human blood CXCR5(+)CD4(+) T cells are counterparts of T follicular cells and contain specific subsets that differentially support antibody secretion. *Immunity* 34:108.
19 King, I. L. and Mohrs, M. 2009. IL-4-producing CD4+ T cells in reactive lymph nodes during helminth infection are T follicular helper cells. *J. Exp. Med.* 206:1001.
20 Glatman Zaretsky, A., Taylor, J. J., King, I. L., Marshall, F. A., Mohrs, M. and Pearce, E. J. 2009. T follicular helper cells differentiate from Th2 cells in response to helminth antigens. *J. Exp. Med.* 206:991.
21 Bryant, V. L., Ma, C. S., Avery, D. T. *et al.* 2007. Cytokine-mediated regulation of human B cell differentiation into Ig-secreting cells: predominant role of IL-21 produced by CXCR5+ T follicular helper cells. *J. Immunol.* 179:8180.
22 Yoon, S. O., Zhang, X., Berner, P. and Choi, Y. S. 2009. IL-21 and IL-10 have redundant roles but differential capacities at different stages of plasma cell generation from human germinal center B cells. *J. Leukoc. Biol.* 86:1311.
23 Hao, Z., Duncan, G. S., Seagal, J. *et al.* 2008. Fas receptor expression in germinal-center B cells is essential for T and B lymphocyte homeostasis. *Immunity* 29:615.
24 Rankin, A. L., Guay, H., Herber, D. *et al.* 2012. IL-21 receptor is required for the systemic accumulation of activated B and T lymphocytes in MRL/MpJ-Fas(lpr/lpr)/J mice. *J. Immunol.* 188:1656.
25 Tada, Y., Koarada, S., Tomiyoshi, Y. *et al.* 2006. Role of inducible costimulator in the development of lupus in MRL/lpr mice. *Clin. Immunol.* 120:179.
26 Zeller, G. C., Hirahashi, J., Schwarting, A., Sharpe, A. H. and Kelley, V. R. 2006. Inducible co-stimulator null MRL-Faslpr mice: uncoupling of autoantibodies and T cell responses in lupus. *J. Am. Soc. Nephrol.* 17:122.
27 Karnell, J. L. and Ettinger, R. 2012. The interplay of IL-21 and BAFF in the formation and maintenance of human B cell memory. *Front. Immunol.* 3:2.
28 Rankin, A. L., MacLeod, H., Keegan, S. *et al.* 2011. IL-21 receptor is critical for the development of memory B cell responses. *J. Immunol.* 186:667.
29 Ozaki, K., Spolski, R., Feng, C. G. *et al.* 2002. A critical role for IL-21 in regulating immunoglobulin production. *Science* 298:1630.
30 Reinhardt, R. L., Liang, H. E. and Locksley, R. M. 2009. Cytokine-secreting follicular T cells shape the antibody repertoire. *Nat. Immunol.* 10:385.
31 Harada, Y., Tanaka, S., Motomura, Y. *et al.* 2012. The 3' enhancer CNS2 is a critical regulator of interleukin-4-mediated humoral immunity in follicular helper T cells. *Immunity* 36:188.
32 Vijayanand, P., Seumois, G., Simpson, L. J. *et al.* 2012. Interleukin-4 production by follicular helper T cells requires the conserved Il4 enhancer hypersensitivity site V. *Immunity* 36:175.
33 Lüthje, K., Kallies, A., Shimohakamada, Y. *et al.* 2012. The development and fate of follicular helper T cells defined by an IL-21 reporter mouse. *Nat. Immunol.* 13:491.
34 Ishida, H., Muchamuel, T., Sakaguchi, S., Andrade, S., Menon, S. and Howard, M. 1994. Continuous administration of anti-interleukin 10 antibodies delays onset of autoimmunity in NZB/W F1 mice. *J. Exp. Med.* 179:305.
35 Kawano, S., Lin, Q., Amano, H. *et al.* 2013. Phenotype conversion from rheumatoid arthritis to systemic lupus erythematosus by introduction of Yaa mutation into FcgammaRIIB-deficient C57BL/6 mice. *Eur. J. Immunol.* 43:770.
36 Lee, S. K., Silva, D. G., Martin, J. L. *et al.* 2012. Interferon-γ excess leads to pathogenic accumulation of follicular helper T cells and germinal centers. *Immunity* 37:880.

37 Bauquet, A. T., Jin, H., Paterson, A. M. *et al.* 2009. The costimulatory molecule ICOS regulates the expression of c-Maf and IL-21 in the development of follicular T helper cells and TH-17 cells. *Nat. Immunol.* 10:167.

38 Zhang, X., Ing, S., Fraser, A. *et al.* 2013. Follicular helper T cells: new insights into mechanisms of autoimmune diseases. *Ochsner J.* 13:131.

39 Atta, A. M., Sousa, C. P., Carvalho, E. M. and Sousa-Atta, M. L. 2004. Immunoglobulin E and systemic lupus erythematosus. *Braz. J. Med. Biol. Res.* 37:1497.

40 Charles, N., Hardwick, D., Daugas, E., Illei, G. G. and Rivera, J. 2010. Basophils and the T helper 2 environment can promote the development of lupus nephritis. *Nat. Med.* 16:701.

41 Maxwell, M. J., Duan, M., Armes, J. E., Anderson, G. P., Tarlinton, D. M. and Hibbs, M. L. 2011. Genetic segregation of inflammatory lung disease and autoimmune disease severity in SHIP-1-/- mice. *J. Immunol.* 186:7164.

42 Bolland, S. and Ravetch, J. V. 2000. Spontaneous autoimmune disease in Fc(gamma)RIIB-deficient mice results from strain-specific epistasis. *Immunity* 13:277.

The Japanese Society
of Gastroenterology

ORIGINAL ARTICLE—ALIMENTARY TRACT

Epithelial-derived nuclear IL-33 aggravates inflammation in the pathogenesis of reflux esophagitis

Jing Shan · Tadayuki Oshima · Taichiro Muto ·
Koubun Yasuda · Hirokazu Fukui ·
Jiro Watari · Kenji Nakanishi · Hiroto Miwa

Abstract

Background IL-33 is a new tissue-derived cytokine constitutively expressed in epithelial cells and plays a role in sensing damage caused by inflammatory diseases. The function of IL-33 in the esophageal mucosa has not been previously described. Accordingly, we examined the expression of IL-33 and its role in the pathogenesis of reflux esophagitis (RE).

Methods IL-33 in the esophageal mucosa of RE patients and in an in vitro stratified normal esophageal squamous epithelial model was examined at the messenger RNA and protein levels. The correlation of the level of IL-33 and IL-8 or IL-6 was examined. Cell layers were stimulated with bile acids and cytokines. IL-33 was knocked down by small interfering RNA (siRNA). Pharmacological inhibitors and signal transducer and activator of transcription 1 (STAT1) siRNA were used.

Results IL-33 was significantly upregulated in RE patients, and was located in the nuclei of basal and suprabasal layers. Upregulated IL-33 messenger RNA

expression was correlated with IL-8 and IL-6 expression. In vitro, IL-33 was upregulated in the nuclei of basal and suprabasal layers by interferon-γ (IFNγ), and the upregulation was aggravated by the combination of deoxycholic acid (DCA) and IFNγ. IL-33 knockdown dampened IFNγ- and DCA-induced IL-8 and IL-6 production. IFNγ-induced IL-33 was inhibited by a Janus kinase inhibitor, a p38 mitogen-activated protein kinase inhibitor, and STAT1 siRNA.

Conclusions Nuclear IL-33 is upregulated in erosive mucosa of RE patients and is correlated with IL-8 and IL-6 levels. The normal esophageal epithelial model enables us to show for the first time that epithelial-cell-derived nuclear but not exogenous IL-33 is located upstream of the production of inflammatory cytokines and can aggravate the inflammation.

J. Shan · T. Oshima (✉) · H. Fukui · J. Watari · H. Miwa
Division of Gastroenterology, Department of Internal Medicine,
Hyogo College of Medicine, 1-1 Mukogawa-cho, Nishinomiya,
Hyogo 663-8501, Japan
e-mail: t-oshima@hyo-med.ac.jp

J. Shan
Department of Gastroenterology, The Third People's Hospital of
Chengdu, Chengdu, China

T. Muto · K. Yasuda · K. Nakanishi
Department of Immunology and Medical Zoology, Hyogo
College of Medicine, Nishinomiya, Japan

Introduction

Recent studies have provided a new view of the pathogenesis of gastroesophageal reflux disease (GERD), namely, that cytokine-mediated rather than direct caustic acid mediated injury causes reflux esophagitis (RE) [1]. Accordingly, several studies have investigated inflammatory mediators in RE and their impact on esophageal motility, fibrosis, and carcinogenesis [2]. Esophageal epithelial cells which are directly exposed to intraluminal stimuli have been shown to produce inflammatory cytokines such as IL-8 and IL-6 following stimulation by acid, bile acid, or trypsin, and these cytokines initiate the inflammation process [3–5]. These data indicated that

esophageal epithelial cells may work not only as a barrier, but may also actively participate in the pathogenesis of RE.

A new tissue-derived cytokine, IL-33, has been described that is constitutively expressed in the endothelial cells and epithelial cells of tissues exposed to the environment [6]. IL-33 acts as both a traditional cytokine and a chromatin-associated nuclear factor in both innate and adaptive immunity [7–10]. The C-terminal IL-1-like cytokine domain of IL-33 can bind to the transmembrane protein ST2, an IL-33 receptor, extracellularly. Binding is followed by activation of nuclear factor κB (NF-κB), then induction of IL-6 and IL-8 in epithelial cells such as keratinocytes [7] and conjunctive epithelial cells [8]. The N-terminal homeodomain-like helix–turn–helix of IL-33 can interact with chromatin, affecting chromatin compaction [9]. A recent study showed that nuclear IL-33 can bind NF-κB directly, thereby regulating gene transcription [10]. Although IL-33 is highly expressed even in the gut [6], and its expression is increased in inflamed tissues in gastrointestinal diseases, such as ulcerative colitis [11, 12], the intracellular function of IL-33 in the gut is unclear and its expression in esophageal epithelial cells has never been studied. Furthermore, whether or not IL-33 participates in the pathogenesis of RE and interacts with other cytokines has never been investigated.

In this study, we investigated the expression and the localization of IL-33 in human esophageal biopsy samples from patients with RE, along with control esophageal tissue. We used a three-dimensional stratified squamous epithelial model using a line of normal human esophageal epithelial cells (HEECs) established by us [13] to investigate the function of IL-33 in esophageal epithelial cells.

Methods

Human endoscopic biopsies

Twenty consecutive patients with visible erosive RE according to the Los Angeles classification and 20 controls matched by age and gender were recruited at Hyogo College of Medicine (between 2012 and 2013) (Table S1). Exclusion criteria for all participants were as follows: intake of nonsteroidal anti-inflammatory drugs, corticosteroids, antiallergic drugs, or other immmunosupressive drugs in the preceding 6 months; allergy or inflammatory bowel diseases. Endoscopic biopsy samples were taken from erosive mucosa of the distal esophagus and unaffected mucosa of the middle (approximately 35 cm from the incisor tooth) esophagus of RE patients and from the distal esophagus of subjects in the control group. One biopsy sample was immediately stored in RNAlater (Qiagen, Hilden, Germany), and was maintained at −20 °C

until the measurement of messenger RNA (mRNA). One biopsy sample for immunofluorescence staining was fixed with 10 % neutral formalin and embedded in paraffin. Patient anonymity was preserved. This study was performed in accordance with the Declaration of Helsinki and was approved by the Ethics Committee/Institutional Review Board of Hyogo College of Medicine, Japan (no. 174). The subjects gave written informed consent.

Reverse transcription quantitative PCR

Total mRNA was extracted according to the manufacturer's instructions using Trizol reagent (Invitrogen Life Technologies, Carlsbad, CA, USA). Contaminated DNA was cleared by RNase-free DNase treatment (Qiagen). Complementary DNA was synthesized using a high-capacity complementary DNA reverse transcription (RT) kit (Applied Biosystems, Foster City, CA, USA). Quantitative PCR (qPCR) was performed using a PCR master mix in a 7900HT fast real-time PCR system (Applied Biosystems). The TaqMan probe and primers for IL-33 (accession no. Hs00369211; Applied Biosystems), IL-8 (accession no. Hs00174103; Applied Biosystems), and IL-6 (accession no. Hs00985639; Applied Biosystems) were assay-on-demand gene expression products. The GAPDH gene (accession no. Hs02758991; Applied Biosystems) was used as the endogenous control. The thermal cycler conditions were as follows: 2 min at 50 °C, 10 min at 95 °C, followed by 40 cycles of 15 s at 95 °C for denaturing and 1 min at 60 °C for annealing/extension. All procedures were repeated in triplicate. Amplification data were analyzed with Sequence Detection System version 2.2 (Applied Biosystems). The $\Delta\Delta C_T$ method recommended by the manufacturer was used to compare the relative expression levels.

Immunofluorescence staining

Paraffin-embedded sections (4 μm thick) of the esophagus were deparaffinized, heated in citrate buffer (pH 6.0) for epitope retrieval, and then cooled at room temperature for 50 min before blocking with phosphate-buffered saline containing 1.0 % bovine serum albumin and 0.05 % Tween 20. The sections were incubated with purified anti-IL-33 polyclonal antibody (rabbit IgG), prepared in our laboratory as described previously [14], at 4 °C overnight. Subsequently, the sections were reacted with biotin-conjugated goat anti-rabbit IgG (Vector Laboratory, Burlingame, CA, USA) at room temperature for 30 min, and were then visualized using AlexaFluor 594 conjugated streptavidin (Life Technologies, Carlsbad, CA, USA) at room temperature for 30 min. After mounting with ProLong Gold antifade mountant with 4',6-diamidino-2-phenylindole (Life Technologies), the sections were examined under a

microscope (Zeiss LSM 510; Carl Zeiss, Thornwood, NY, USA). Computer software (ZEN 2011; Carl Zeiss) was used for image processing and analysis.

The fluorescence intensity of IL-33 was determined by measuring the average pixel intensity in a region of interest using ZEN 2011. Each average pixel intensity value was corrected for the background intensity, and then the mean intensity of three sections per sample was used as the average intensity. The evaluation was done by two independent observers (K.Y., T.M.) blinded to the group assignment.

Cell culture

HEECs were purchased from ScienCell Research Laboratories (Carlsbad, CA, USA). For air–liquid interface (ALI) culture, Transwell clear wells (Costar, Cambridge, MA, USA) were coated with collagen, human fibronectin, and bovine serum albumin. The cells were cultured in epithelial cell medium-2 (ScienCell Research Laboratories) and subcultured in Transwell clear wells until approximately 80 % confluence. ALI culture was then conducted as described in detail previously [13, 15, 16]. The stratified squamous epithelial model was ready after 10 days of ALI culture. For monolayer culture, HEECs were cultured in epithelial cell medium-2 in a 96-well plate. Passages 3–7 were used for this study.

Reagents

Interferon-γ (IFNγ), IL-1β, TNF-α, and IL-33 were purchased from R&D Systems (Minneapolis, MN, USA). Deoxycholic acid (DCA) was purchased from Wako Pure Chemical Industries (Tokyo, Japan). Chenodeoxycholic acid (CDCA) was purchased from Sigma (St Louis, MO, USA). Soluble ST2 (sST2) was purchased from Enzo Life Sciences (Farmingdale, NY, USA). JAK inhibitor I (an inhibitor or Janus kinases), SB203580 [a p38 mitogen-activated protein kinase (MAPK) inhibitor], and H89 [a protein kinase A (PKA) inhibitor] were purchased from Calbiochem (Milan, Italy). Epigallocatechin gallate (EGCG) [a signal transducer and activator of transcription 1 (STAT1) inhibitor] was purchased from Wako Pure Chemical Industries Ltd.

Construction of experimental model and various treatments

In the ALI-cultured model, each well had an apical and basal compartment; the apical compartment represented the luminal side of the esophagus, whereas the basal compartment represented the subepithelial side. Cells were incubated in serum-free medium without bovine pituitary extract for 24 h before stimulation. HEECs were stimulated

from the basal compartment by IFNγ (30 ng/ml), IL-1β (10 ng/ml), and TNF-α (20 ng/ml), or from the apical compartment by acidified growth medium (pH 1, 2), acidic DCA (400 μM, pH 6.5), and acidic CDCA (400 μM, pH 6.5) for the indicated time. Blocking experiments were performed by preincubation with JAK inhibitor I (0.2–2 μM), SB203850 (20–40 μM), and EGCG (20 μM) from the basal compartment for 60 min. IFNγ (30 ng/ml) was then added to the basal compartment for the indicated time in the presence of pretreatment inhibitors. Each experiment was performed in triplicate.

Western blot analysis

Cells were collected after stimulations, and the protein was extracted by reduced lysis buffer [60 mM tris(hydroxy-methyl)aminomethane–HCl (pH 6.8), 10 % glycerol, one tablet of protein inhibitor] for the total fraction. Protein concentrations were determined by a Bradford assay kit (Bio-Rad Laboratories, Hercules, CA, USA) according to the manufacturer's instructions.

Equal quantities of protein were separated by electrophoresis on 10 % sodium dodecyl sulfate–polyacrylamide gel electrophoresis gels. Gels were transferred to nitrocellulose membranes (Hybond ECL; GE Healthcare UK, Little Chalfont, UK). The membrane was incubated with goat anti-IL-33 (R&D Systems) at 1:1,000 or mouse anti-β-actin (Cell Signaling) at 1:1,000 overnight at 4 °C. After the incubation with the appropriate secondary horseradish peroxidase conjugated IgG antibody (R&D Systems) for 2 h at room temperature, the membrane was detected with an ECL-Plus western blot detection system (GE Healthcare UK) according to the manufacturer's instructions. All experiments were performed at least three times. The results of a typical experiment are shown. The western blot bands were analyzed by ImageJ (Bio-Arts, Fukuoka, Japan).

Measurement of cytokines

IL-8 enzyme-linked immunosorbent assay (ELISA) (KHC0081; Invitrogen), IL-6 ELISA (KHR0061; Invitrogen), and Bio-Plex human cytokine 27-plex panel (Bio-Rad Laboratories) were used according to the manufacturers' instructions to measure the levels of cytokines and chemokines. Medium in the basal compartment in the ALI-cultured model and the culture supernatant in the monolayer model was centrifuged to remove cellular debris, and was then stored at −80 °C until analysis.

Small interfering RNA

For small interfering RNA (siRNA) silencing, human IL-33 and STAT1 ON-TARGETplus SMARTpool siRNA,